STRESSES IN BEAMS WITH CIRCULAR ECCENTRIC WEB HOLES

by

Peter W. Chan and Richard G. Redwood

Structural Mechanics Series No. 73-3

March 1973

STRUCTURES LABORATORY

McGILL UNIVERSITY

DEPARTMENT OF CIVIL ENGINEERING AND APPLIED MECHANICS

MONTREAL, CANADA

Stresses in Beams with Circular Eccentric Web Holes

by

Peter W. Chan[a], A.M.ASCE and Richard G. Redwood[b]

INTRODUCTION

The stress analysis of beams containing web holes has received considerable attention because of the frequency of occurrence of such holes in building construction. While plastic design methods may be preferred because of their rationality, and their application to rectangular holes has been explored extensively, the allowable stress approach to design may be necessary in some cases. In particular, holes in non-compact sections require elastic analysis, and the treatment of circular holes by plastic design methods is currently less satisfactory than rectangular holes.[3] The stress concentrations produced by circular holes are much lower than those produced near the corners of rectangular holes, and whereas the latter will normally produce local yielding under working loads, the former may be low enough that stresses under working loads can be kept within permissible limits.

Much of the previous work directed to the analysis of webs with circular holes has been restricted to mid-depth holes. It is probable that designers are more frequently concerned with the case of eccentric holes than with mid-depth holes, since service ducts or piping may well be located at different levels between floors to facilitate any crossing which may be necessary. Analysis of eccentrictric holes is therefore of considerable importance.

---

a) Graduate Student, Department of Civil Engineering & Applied Mechanics, McGill University, Montreal, Canada.

b) Associate Professor & Chairman, Department of Civil Engineering & Applied Mechanics, McGill University, Montreal, Canada.

The avoidance of fabricating reinforcement is desirable on the basis of cost, and it is therefore of some importance to determine the stress levels around unreinforced holes. While some specifications[9] permit unreinforced circular holes, subject to certain size and location limitations, without the need for analysis, these are, of necessity, quite restrictive. In this paper, more general conditions are considered, so that any practical sized circular web hole can be investigated in terms of the maximum stresses it produces.

Much previous analytical work concerning such holes has made use of the theory of elasticity in analysing the web as a large plate containing a small hole,[1,6] and in addition, emphasis has been placed on mid-depth holes, although an outline of an analytical procedure for eccentric holes has been given in Reference 6. The accuracy of the theory of elasticity solution has been investigated by Bower[1,2] and it is clear that the method is seriously deficient under some circumstances, in particular for large holes and under high shear-to-moment ratios, both of which frequently arise in practise. Alternative approaches, for mid-depth holes, have been proposed in which parts of the beam around the hole have been treated as frame members, and analysed by elementary beam theory,[7] with the inclusion of stress concentration factors to account for the curved edge.

The two approaches, theory of elasticity and curved beam analysis, are compared herein for mid-depth holes, and the conditions under which each is most appropriate are determined. The approximate approach is then extended to deal with eccentric holes by considering the division of shear between the parts of the beam above and below the hole. Experiments on large mid-depth holes and eccentric holes are described, and results compared with the analytical solution. Previous experimental results obtained elsewhere[5] are also used for comparison. Finally, design aids in the form of moment-shear interaction diagrams are presented which relate specifically to maximum stress conditions on the hole edges and in the flanges.

ANALYSIS

The two approaches are outlined below for mid-depth holes and eccentric holes. The relevant method to use is discussed in a subsequent section, in the light of experimental results.

Mid-Depth Holes

Theory of Elasticity Solution

This theory is outlined in References (1) and (6). A useful explicit relationship for the tangential normal stress on the edge of a

hole is given by equation (6) in Reference 1. For the specific case of a circular hole, this reduces to:

$$\frac{\sigma_t}{F_b} = \frac{M}{M_{all}}\left(\frac{2R}{d}\right)(\sin\beta - \sin 3\beta) + 4\left(\frac{M}{M_{all}}\right)\left(\frac{\tau}{\sigma}\right)\Gamma \sin 2\beta \qquad (1)$$

where σ_t = the tangential normal stress on the hole edge, F_b = the allowable bending stress, M = the applied moment at the hole centreline, M_{all} = the allowable being moment based on F_b and the gross section of the beam, R = the hole radius, d = the overall beam depth, β = the angle measured from the horizontal through the hole centre, τ = the nominal average shear stress based on the gross web area, σ = the nominal bending stress at the outside fibre of the beam, again based on gross section, and Γ = the ratio of the maximum nominal shear stress to τ. Explicit relationships for stresses in other locations are not available. The above equation is valid for small holes only, except that if the shear-to-moment ratio is low, holes with diameter equal to or somewhat larger than one half the hole depth may be analysed with satisfactory results. For large holes especially if the shear-to-moment ratio is not low, the following analysis is proposed.

Curved Beam Analysis

In this analysis parts of the beam near the hole are treated as individual structural members, and analysed accordingly by well established methods. The resultant forces acting on a cross-section of the beam through the centre of the hole, as shown in Figure 1, are first estimated. Symmetry requires that half of the total shear force be carried above the hole, and the magnitude and line of action of the normal force N can be approximated by application of the simple fle-

xure formula. This can be based on the moment applied at the centreline of the hole, and the properties of the net section at that location. Stresses are then calculated for several sections radiating from the hole centre, as indicated. The normal force acting through the centroid of such a section and the moment, N_ϕ and M_ϕ, are then used to calculate the stresses.

The stresses due to bending may be calculated on the assumption that the section defined by the angle ϕ is the cross section of a curved beam with centre of curvature at the centre of the hole. Then using the Winkler-Bach curved beam formula[8] the bending stress at the edge of the hole is

$$\sigma_b = \frac{M_\phi}{A(R + c)} \left(1 - \frac{c}{ZR}\right) \tag{2}$$

where $$Z = -\frac{1}{A} \int_{\text{area}} \frac{y}{(R + c) + y} \, dA \, , \tag{3}$$

A = area of the inclined tee-section defined by the angle ϕ, c = the distance from the hole edge to the centroid of the inclined tee, and y = a coordinate measured from the centroid of the inclined tee-section.

The integration of equation (3) may be performed numerically, or alternatively explicit formulae are given for a number of different section shapes in Reference (8). In particular, for a tee section as shown in figure 2,

$$Z = -1 + \frac{R+c}{A} \left[b \, \ell n(R+c+u_1) + (w-b) \, \ell n(R+c+u_2) - w \, \ell n(R)\right] \tag{4}$$

It is convenient to calculate a stress concentration factor K for the hole edge stress based on equation (2). Thus,

$$K = \frac{\frac{M_\phi}{A(R+c)} \left(1 - \frac{c}{ZR}\right)}{\frac{-M_\phi c}{I}} \tag{5}$$

where I is the moment of inertia of the inclined tee-section about its centroid.

The stress caused by N_ϕ must be added to the bending component, and it has been found sufficiently accurate to apply the same stress concentration factor K to the nominal axial stress value as derived by consideration of the bending stresses. Thus the tangential stress at the hole edge becomes

$$\sigma_t = K\left(\frac{N_\phi}{A} + \frac{M_\phi c}{I}\right) \tag{6}$$

This calculation is repeated for various values of ϕ until a maximum value of σ_t is reached. This process can be carried out up to a maximum ϕ of about 45°, and it has been found that for practical hole and beam geometries, the maximum always occurs with $\phi < 45°$.

Eccentric Holes

Theory of Elasticity Solution

The theory is outlined in Reference (6) and the following explicit relationship for the hole edge stress for circular holes may be derived:

$$\frac{\sigma_t}{F_b} = \frac{M}{M_{all}}\left(\frac{2R}{d}\right)(\sin\beta - \sin 3\beta) + 4\left(\frac{M}{M_{all}}\right)\left(\frac{T}{\sigma}\right)\Gamma \sin 2\beta$$

$$+ \quad 2\left(\frac{M}{M_{all}}\right)\left(\frac{e}{d}\right)(1 - 2\cos 2\beta) - \frac{1}{2}\left(\frac{V}{V_{all}}\right)\left(\frac{F_v}{F_b}\right)\left(\frac{e}{d}\right)\left(\frac{A_w}{A_f}\right)$$

$$\left(\frac{A_f d^2}{I}\right)\left(\frac{2R}{d}\right)\left[\cos\beta - 3\cos 3\beta + 4\,\frac{e}{d}\left(\frac{d}{2R}\right)\sin 2\beta\right] \tag{7}$$

where e = the eccentricity measured as the distance from the centre of the hole to the beam centreline, V = the total shear, V_{all} = the allowable shear, F_v = the allowable shear stress, A_w = the gross web area (= dw), and A_f = the area of one flange.

Curved Beam Solution

This method follows the identical procedure as for the mid-depth hole, the only difference being that the shear force is no longer distributed equally

above and below the hole. In order to calculate the division of shear, the sections of the beam above and below the hole are treated separately, and conditions of slope and deflection compatibility between their ends are employed.

Equilibrium requires that the sum of shear forces in the upper and lower sections must be equal to the total shear force at hole centreline, V, that is,

$$V_T + V_B = V \tag{8}$$

where V_T and V_B = the shear forces in the upper and lower sections respectively. From slope and deflection compatibility, that is, equality of the changes in slope and deflection of the upper and lower sections over the length of the hole, the following shear force ratio is obtained:

$$\frac{V_T}{V_B} = \frac{\frac{R^2}{E}\int_0^{\frac{\Pi}{2}} \frac{\sin^2\theta \cos\theta d\theta}{I_B} + \frac{1}{G}\int_0^{\frac{\Pi}{2}} k_B \cos\theta d\theta}{\frac{R^2}{E}\int_0^{\frac{\Pi}{2}} \frac{\sin^2\theta \cos\theta d\theta}{I_T} + \frac{1}{G}\int_0^{\frac{\Pi}{2}} k_T \cos\theta d\theta} \tag{9}$$

where E = Young's Modulus, I_T, I_B = the moments of inertia of upper and lower sections respectively about their centroids, θ = an angle measured from the centre of the hole from its vertical centreline, G = shear modulus, and k_T, k_B = shear stress parameters for the upper and lower sections respectively. A detailed analysis of the derivation of equation 9 is given in Appendix I.

In order to verify the above theories, and to determine which is the more appropriate to use in a given case, some experiments were performed, and are described in the next section.

TEST PROGRAM AND RESULTS

Two beams each containing two holes were tested to determine elastic stress distributions and deflections. Details of the beams, holes and test arrangements are shown in Figure 3. The two holes in Beam A were chosen to be large enough that the theory of elasticity solution would almost certainly be inadequate for their analysis, and the results therefore represent a test of the curved beam method of analysis. The smaller holes of Beam B were chosen in an attempt to explore the limitations in application of the two analytical approaches. All holes were tested under two different shear-to-moment ratios, since the adequacy of the analytical approaches is known to be very dependent on this ratio.

The holes were machined with a fly cutter, and thus had clean, notch free edges. While in practice most holes would be flame cut, the resulting stress raisers would in fact be ignored by the designer, unless fatigue was a consideration. It was therefore preferred to eliminate the effects of a rough edge and so provide a clearer picture of the relevance of the analyses. The webs and flanges of the beams in the vicinity of each hole were strain gauged, and gauge locations are shown on Figure 4.

The beams were simply supported at each end, and because of the low magnitudes of load, no lateral support was provided. Load was applied by means of an Amsler hydraulic jack and readings of gauges and deflections recorded at a minimum of 5 increments of load. A maximum load of 13 kips was applied to Beam A, and 21 kip to Beam B, and no non-linearity was observed in any of the readings. The beams were tested with the holes in the positions shown in Figure 3, and then with the reversed position with the holes eccentric below the mid-depth. Much of the data was automatically recorded and stored on disk for later analysis.

Tangential normal stresses around the hole edge are shown on Figures 5 to 8. Also plotted are solutions given by the theory of elasticity and by the curved beam method; for the latter, stresses are plotted only for the sector $\pm$ 45° from the vertical centre-line of the hole, because of the limitation of the method. Stresses around the large holes of Beam A are shown on Figures 5 and 6 for M/V = 24 in. In both cases, the theory of elasticity solution is quite inadequate, and the curved beam solution accurately predicts the measured stresses. Similar results were also obtained for these holes under a M/V ratio of 48 in. Results for Hole 3 of Beam B are shown in Figure 7 for the two M/V ratios. Under the lower M/V ratio, the two analyses give very close results, and both predict the measured stresses well. At the higher M/V ratio, the theory of elasticity solution provides a good estimate of the measured stresses while the accuracy of the curved beam results is diminished. Similar conclusions can be drawn from the results for Hole 4, shown on Figure 8. These results are consistent with the known dependence of both methods on the M/V ratio.

Shear stresses were measured by rosette gauges placed on the hole centreline. Experimental results are shown for two M/V ratios on Figures 9 and 10, and are compared with the theoretical stress distributions based on the shear force values given by equations (8) and (9) with the distribution according to standard elastic theory. Satisfactory agreement was found in all cases.

Longitudinal normal stresses were measured on the centreline of the flanges at various positions over the length of the hole. Typical values are shown in Figures 11 and 12, and are compared with values obtained in the following two ways: flexural stresses calculated from the applied bending moment, and based on the gross (i.e. unperforated) beam section modulus, and values of flange stresses obtained from the curved beam analysis. The latter were calculated on planes $\pm$ 45° from the hole centreline, and it can be expected that the accuracy will diminish as the angle increases. The results in general do not

show great deviations from the nominal stress values, except in cases where the hole is very large or the eccentricity is large. In either case, it can be expected that the maximum hole edge stress will be large, and might in any case govern. The curved beam estimates of the longitudinal flange stresses generally indicate the stress distributions, and predict the maximum values quite well although the location is generally not predicted accurately.

Four W16 x 40 beams of A36 steel containing eccentric circular holes were tested by Frost.[5] The holes were 6.4 in. diameter, and eccentricities were 1.0 in. and 2.0 in. Stresses were measured on three cross sections of the beam corresponding to the centreline and the two ends of the hole. However, strains were not recorded at the edges of the holes other than at these sections. Thus only the stresses at the hole centreline can be compared with the theories herein. Shear stresses at this location again showed good agreement between the theory and experiment as shown on Figure 13.

DESIGN AIDS

For the experimental cases presented herein, it has been shown that, depending upon the hole size and the M/V ratio, either the curved beam method or the theory of elasticity method gives a satisfactory solution for the maximum hole edge stress. The appropriate solution is always the one predicting the greater stress magnitude. It is therefore apparent that for a given case, if both solutions are obtained, the larger stress predicted may be taken as the more accurate; however, it has not been demonstrated that such a result will be sufficiently accurate for all practical values of M/V and 2R/d.

A study of the accuracy of the two methods in predicting the maximum hole edge stress for mid-depth holes has been presented in Reference 4. For a number of reported results of experiments and finite element analyses of mid-depth holes, the maximum stresses predicted by the two analyses have been compared, and non-dimensionalised stresses plotted against a non-dimensional parameter M/Vd, representing the moment-to-shear ratio. Results for the smallest hole (2R/d = .434) and the largest one (2R/d = 0.758) are shown on Figure 14. These and other results showed that taking the largest of the two stresses could result in unsafe prediction of the actual stress, with a maximum underestimate of about 14%. This however applies only over a limited range of M/Vd ratios, and only to small holes, for which stress levels elsewhere in the beam may well be critical. Thus for most purposes, the largest value of stress given by the two methods may be considered sufficiently accurate.

On this basis, design aids have been prepared and are given in Figures 16 to 27. It has been assumed that the above conclusions arrived at for mid-depth holes hold equally for eccentric holes, and therefore the effects of eccentricity are included in these diagrams.

The diagrams take the form of interaction curves relating the shear force V and moment M which, acting together will just cause the maximum hole edge stress to reach the allowable value. Thus values of M and V which just cause the maximum stress to reach F_b are represented by points on the curve, and points on the concave side of the boundary represent lower values of the maximum stress. Points outside the curve represent unsafe load combinations. Shear and moment have been non-dimensionalised by dividing by V_{all} and M_{all} respectively, these being the allowable values of shear and moment, based on the nominal gross beam section. It has been assumed that $F_v = 2F_b/3$ where F_v and F_b are the allowable shear and bending stress respectively. In addition it has been assumed that $t/d = 0.05$ and $A_w/A_f = 2.0$; the results are not sensitive to these ratios, and the assumed values both lead to slightly conservative results.

For all these diagrams, maximum flange stresses given by the curved beam analysis have been calculated, and in a few cases, corresponding to small holes with small or zero eccentricity, under low shear forces these were found to be critical. The interaction diagrams take these flange stresses into account, as indicated on Figure 15. This diagram shows four regions of the diagram, one corresponding to the case when flange stresses govern, and the other three to hole edge stresses. A typical diagram will contain two or more of these zones.

Figures 16 to 27 provide design aids for most practical situations, and account for the effects of the hole on normal stresses in both flange and web. The remaining check which a designer must make concerns the maximum shear stress. As an aid to this, Figure 28 gives the division of shear force above and below the hole. Because these values are dependent upon A_w/A_f, although not very sensitively, results are given for $A_w/A_f = 0.75$ and 2.0, and intermediate values may be obtained by interpolation. This may be used to calculate the shear stresses in the top and bottom tee sections on the hole centreline.

EXAMPLE

Given the beam dimensions and loading shown on Figure 29, it is required to check the adequacy of the beam if a hole of 9 inch diameter and eccentricity 2 inch is placed 6 ft. from the left hand support. The beam is laterally supported along the span and has a yield stress of 50 ksi (A441 steel).

Since the beam is non-compact, $F_b = 0.60\ F_y = 30$ ksi

$$F_v = 0.40\ F_y = 20 \text{ ksi}$$

Maximum bending moment at mid-span $= \frac{40 \times 20 \times 12}{4} = 2400$ k-in.

Maximum bending stress $= \frac{2400 \times 18.0}{2 \times 802} = 26.93 \text{ ksi} < F_b$ O.K.

Hole diameter to beam-depth ratio $(\frac{2R}{d}) = \frac{9}{18} = 0.5$

Eccentricity to beam-depth ratio $(\frac{e}{d}) = \frac{2}{18} = 0.11$

Moment at hole centreline M = 20 x 6 x 12 = 1440 k-in.

Shear at hole centreline V = 20 kips

Allowable Moment $M_{all} = \frac{30 \times 2 \times 802}{18} = 2673.3$ k-in.

Allowable Shear $V_{all} = 20 \times 18 \times .358 = 128.8$ kips

$$\frac{M}{M_{all}} = \frac{1440}{2673.3} = .54 \qquad \frac{V}{V_{all}} = \frac{20}{128.8} = .16$$

This point is plotted on Figure 29 and is found to be in the safe region.

Shear stress at hole centreline

Interpolating from Figure 28,

$$V_T = .26V = 5.2 \text{ kips}$$

$$V_B = .74V = 14.8 \text{ kips}$$

The locations of the neutral axis for the top and bottom tee sections are given in Figure 31.

Moment of inertia of top tee section, $I_T = 1.26$ in.^{4}

Moment of inertia of bottom tee section, $I_B = 21.32$ in.^{4}

Maximum shear stress in top tee $= \frac{V_T Q_T}{I_T w}$

$$= \frac{5.2 \times 1.93 \ (2.041 - \frac{1.93}{2})}{1.26}$$

$$= 8.57 \text{ ksi} < F_v \qquad \text{O.K.}$$

Maximum shear stress in bottom tee $= \frac{V_B Q_B}{I_B w}$

$$= \frac{14.8 \times 5.137^2}{21.32 \times 2}$$

$$= 9.16 \text{ ksi} < F_v \qquad \text{O.K.}$$

Hence the stresses at the hole are within allowable limits.

ACKNOWLEDGEMENT

The work described herein was supported by the National Research Council of Canada, under Grant A-3366. Acknowledgement is also made to the Dominion Bridge Company, Montreal, who provided support for one of the authors (PWC) by a Dominion Bridge Fellowship award.

APPENDIX I - SHEAR FORCE DIVISION

The division of shear force V between the unequal top and bottom sections across the web hole can be determined by assuming that the deflections and slopes of the top and bottom sections are equal.[5] Using the Moment Area Method, the deflections and change in slopes of the high moment end of the hole with respect to the low moment end, or vice versa, can be calculated. The free-body diagram, the bending moment diagram and the M/EI diagram for a typical top section are given in Figure 30.

Deflections and Slopes

With the coordinate system indicated in Figure 30. the deflections and slopes due to bending and shear for the top and bottom sections are given as follows:

	Deflection	Slope
Bending (top section)	$\int_o^{2R} \frac{M_T^1 \, x}{EI_T} dx - \int_o^{2R} \frac{V_T x^2}{EI_T} dx$	$\int_o^{2R} \frac{M_T^1}{EI_T} dx - \int_o^{2R} \frac{V_T x}{EI_T} dx$
Shear (top section)	$-\int_o^{2R} \frac{\tau_{T,max}}{G} dx$	$-\int_o^{2R} \frac{d\tau_{T,max}}{G}$
Bending (bottom section)	$\int_o^{2R} \frac{M_B^1 \, x}{EI_B} dx - \int_o^{2R} \frac{V_B x^2}{EI_B} dx$	$\int_o^{2R} \frac{M_B^1}{EI_B} dx - \int_o^{2R} \frac{V_B x}{EI_B} dx$
Shear (bottom section)	$-\int_o^{2R} \frac{\tau_{B,max}}{G} dx$	$-\int_o^{2R} \frac{d\tau_{B,max}}{G}$

Sectional Properties

It is convenient to express the sectional properties, area and moment of inertia, in polar coordinates (r,θ) rather than the cartesian coordinates (x,y). With reference to Figure 31, the transformation equations are:

$$x = R(\sin\theta + 1) \tag{10}$$

and

$$y = R\cos\theta \tag{11}$$

From Figure 31, it can be shown that for any section n-n,

$$\ell_T^o = \frac{d}{2} - t - e \ ,$$

$$\ell_T = \ell_T^o - R\cos\theta \ ,$$

$$A_T = bt + w\ell_T \ ,$$

$$\bar{C}_T = \left[bt\left(\ell_T + \frac{t}{2}\right) + \frac{w\ell_T^2}{2}\right]/A_T \ ,$$

and

$$I_T = \frac{bt^3}{12} + bt\left(\ell_T + \frac{t}{2} - \bar{C}_T\right)^2 + \frac{w\ell_T^3}{12} + w\ell_T\left(\bar{C}_T - \frac{\ell_T}{2}\right)^2$$

where t = flange thickness, A_T = sectional area, b = flange width, w = web thickness, $\bar{C}_T$ = the distance of the neutral axis from the hole edge, and I_T = the moment of inertia of the section.

For the location of the maximum shear stress, and its magnitude, $\tau_{T,max}$ two cases need to be considered, namely, when the neutral axis lies in the web and in the flange.

When neutral axis lies on the web:

$$\tau_{T,max} = \frac{V_T\bar{C}_T^2}{2I_T} \tag{12}$$

and when neutral axis lies on the flange:

$$\tau_{T,max} = \frac{V_T\left(\bar{C}_T - \frac{\ell_T}{2}\right)}{I_T} \tag{13}$$

In general, $\tau_{T,max}$ can be expressed as:

$$\tau_{T,max} = k_T V_T \tag{14}$$

Equating the Deflections and Slopes

By equating the deflection and slope of the top and bottom section, the following equations are obtained:

$$\int_o^{2R} \frac{M_T^1 x}{EI_T}\,dx - \int_o^{2R} \frac{V_T x^2}{EI_T}\,dx - \int_o^{2R} \frac{\tau_{T,max}}{G}\,dx$$

$$= \int_o^{2R} \frac{M_B^1 x}{EI_B}\,dx - \int_o^{2R} \frac{V_B x^2}{EI_B}\,dx - \int_o^{2R} \frac{\tau_{B,max}}{G}\,dx \qquad (15)$$

$$\int_o^{2R} \frac{M_T^1}{EI_T}\,dx - \int_o^{2R} \frac{V_T x}{EI_T}\,dx - \int_o^{2R} \frac{d\tau_{T,max}}{G}$$

$$= \int_o^{2R} \frac{M_B^1}{EI_B}\,dx - \int_o^{2R} \frac{V_B x}{EI_B}\,dx - \int_o^{2R} \frac{d\tau_{B,max}}{G} \qquad (16)$$

The above equations, (15) and (16), can be rewritten in polar coordinates using equations (10), (11) and (14) as:

$$\int_{-\frac{\pi}{2}}^{\frac{\pi}{2}} \frac{M_T^1}{EI_T} R(\sin\theta + 1) R\cos\theta d\theta - \int_{-\frac{\pi}{2}}^{\frac{\pi}{2}} \frac{V_T}{EI_T} R^2(\sin\theta + 1)^2 R\cos\theta d\theta - \int_{-\frac{\pi}{2}}^{\frac{\pi}{2}} \frac{V_T k_T}{G} R\cos\theta d\theta$$

$$= \int_{-\frac{\pi}{2}}^{\frac{\pi}{2}} \frac{M_B^1}{EI_B} R(\sin\theta + 1) R\cos\theta d\theta - \int_{-\frac{\pi}{2}}^{\frac{\pi}{2}} \frac{V_B}{EI_B} R^2(\sin\theta + 1)^2 R\cos\theta d\theta - \int_{-\frac{\pi}{2}}^{\frac{\pi}{2}} \frac{V_B k_B}{G} R\cos\theta d\theta \qquad (17)$$

$$\int_{-\frac{\pi}{2}}^{\frac{\pi}{2}} \frac{M_T^1}{EI_T} R\cos\theta d\theta - \int_{-\frac{\pi}{2}}^{\frac{\pi}{2}} \frac{V_T R(\sin\theta + 1)}{EI_T} R\cos\theta d\theta - \int_{-\frac{\pi}{2}}^{\frac{\pi}{2}} \frac{V_T}{G} dk_T$$

$$= \int_{-\frac{\pi}{2}}^{\frac{\pi}{2}} \frac{M_B^1}{EI_B} R\cos\theta d\theta - \int_{-\frac{\pi}{2}}^{\frac{\pi}{2}} \frac{V_B R(\sin\theta + 1)}{EI_B} R\cos\theta d\theta - \int_{-\frac{\pi}{2}}^{\frac{\pi}{2}} \frac{V_B}{G} dk_B \qquad (18)$$

On expansion, many of the integrals are found to be odd functions, and therefore vanish. Rearrangement of these equations then leads to the following

$$\frac{M_T^1 R}{E} \int_o^{\frac{\pi}{2}} \frac{\cos\theta d\theta}{I_T} - \frac{V_T R^2}{E} \int_o^{\frac{\pi}{2}} \frac{\sin^2\theta\cos\theta d\theta}{I_T} - \frac{V_T R^2}{E} \int_o^{\frac{\pi}{2}} \frac{\cos\theta d\theta}{I_T} - \frac{V_T}{G} \int_o^{\frac{\pi}{2}} k_T \cos\theta d\theta$$

$$= \frac{M_B^1 R}{E} \int_0^{\frac{\Pi}{2}} \frac{\cos\theta d\theta}{I_B} - \frac{V_B R^2}{E} \int_0^{\frac{\Pi}{2}} \frac{\sin^2\theta \cos\theta d\theta}{I_B} - \frac{V_B R^2}{E} \int_0^{\frac{\Pi}{2}} \frac{\cos\theta d\theta}{I_B} - \frac{V_B}{G} \int_0^{\frac{\Pi}{2}} k_B \cos\theta d\theta \quad (19)$$

$$\frac{M_T^1 R}{E} \int_0^{\frac{\Pi}{2}} \frac{\cos\theta d\theta}{I_T} - \frac{V_T R^2}{E} \int_0^{\frac{\Pi}{2}} \frac{\cos\theta d\theta}{I_T} = \frac{M_B^1 R}{E} \int_0^{\frac{\Pi}{2}} \frac{\cos\theta d\theta}{I_B} - \frac{V_B R^2}{E} \int_0^{\frac{\Pi}{2}} \frac{\cos\theta d\theta}{I_B} \quad (20)$$

Equations (19) and (20) can thus be solved simultaneously to yield equation (9), which can be integrated numerically to provide values of V_T/V_B.

APPENDIX II - REFERENCES

1. Bower, John E., *Elastic Stresses Around Web Holes in Wide-Flange Beams, Journal of the Structural Division,* ASCE, Vol. 92, No. ST2, Proc. Paper 4773, April, 1966, pp 85-101.
2. Bower, John E., *Experimental Stresses in Wide-Flange Beams With Holes, Journal of the Structural Division,* ASCE, Vol. 92, No. ST5, Proc. Paper 4945, October, 1966, pp 167-186.
3. Bower, John E., (Chairman), Subcommittee on Beams with Web Openings of the Task Committee on Flexural Members of the Structural Division, *Suggested Design Guides For Beams With Web Holes, Journal of the Structural Division,* ASCE, Vol. 97, No. ST11, Proc. Paper 8536, Nov., 1971, pp 2707-2728.
4. Chan, P.W., *Approximate Methods to Calculate Stresses Around Circular Holes, Report to Canadian Institute of Steel Construction,* Project 695, Nov., 1971.
5. Frost, R.W., *The Behaviour of Steel Beams With Eccentric Web Holes, Paper presented at ASCE Conference,* St. Louis, Missouri, October, 1971.
6. Heller, S.R. Jr., Brock, J.S., and Bart, R., *The Stresses Around A Rectangular Opening With Rounded Corners In A Beam Subjected To Bending With Shear, Proceedings, 4th U.S. National Congress of Applied Mechanics,* ASME, Vol. 1, 1962, pp 489-496.
7. Sahmel, D., *Konstruktive Ausbildung and Näherungsberechnung geschweisster Biegeträger und Torsionsstäbe mit grossen Stegausnehmungen, Schweissen and Schneider,* 1969, No. 4, (The Design, Construction and Approximate Calculation of Welded Transverse Beams and Torsion Bars Having Pronounced Web Clearance).
8. Seely, F.B., and Smith, J.O., *Advanced Mechanics of Materials,* 2nd ed., Wiley, 1967.
9. *Steel Structures for Building, Canadian Standards Association,* Standard S16-1969.

APPENDIX III - NOTATION

The following symbols are used in this paper:

A = area of inclined tee-section defined by angle ϕ;

A_f = area of one flange;

A_T = area of vertical top tee-section;

A_w = area of web;

b = width of flange;

c = distance from the hole edge to the centroid of the inclined tee-section;

$\bar{c}_T$ = distance from the hole edge to the centroid of the vertical top tee-section;

d = overall depth of beam;

E = Young's Modulus;

e = eccentricity with respect to the beam centreline;

F_b = allowable bending stress;

F_v = allowable shear stress;

F_y = yield stress of steel;

G = shear modulus;

I = moment of inertia of the inclined tee-section;

I_B = moment of inertia of the vertical bottom tee-section;

I_T = moment of inertia of the vertical top tee-section;

K = stress concentration factor;

k_B = shear stress parameter for vertical bottom tee-section;

k_T = shear stress parameter for vertical top tee-section;

M = moment at hole centreline;

M_{all} = allowable bending moment based on F_b and the gross section of the beam;

M_ϕ = resulting moment in inclined tee-section;

M_B^1 = bending moment at bottom tee-section (high moment edge of hole);

M_B^2 = bending moment at bottom tee-section (low moment edge of hole);

M_T^1 = bending moment at top tee-section (high moment edge of hole);

M_T^2 = bending moment at top tee-section (low moment edge of hole);

N = normal force at hole centreline;

N_ϕ = resulting normal force at inclined tee-section;

Q_B = first moment of area about centroid of bottom tee-section;

Q_T = first moment of area about centroid of top tee-section;

R = hole radius;

t = flange thickness;

u_1 = distance of flange from the neutral axis of inclined tee-section;

u_2 = distance of the web-flange interface from the neutral axis of inclined tee-section;

V = shear force at hole centreline;

V_{all} = allowable shear based on F_v and the gross section of the beam;

w = web thickness;

Z = property of area;

β = angle measured from the horizontal through the hole centre;

ϕ, θ = angles measured from the vertical through the hole centre;

τ = nominal average shear stress based on gross web area;

$\tau_{B,max}$ = maximum shear stress of vertical bottom tee-section;

$\tau_{T,max}$ = maximum shear stress of vertical top tee-section;

Γ = ratio of maximum nominal shear stress to τ;

σ = nominal bending stress at outside fibre of the beam based on gross section;

σ_b = bending stress at hole edge;

σ_t = the tangential stress at hole edge;

ℓ_T = length of web of any vertical top tee-section; and

ℓ_T^o = length of web of vertical top tee-section at hole ends.

FIGURE CAPTIONS

FIG. 1 - CURVED BEAM IDEALIZATION

FIG. 2 - TYPICAL INCLINED TEE-SECTION

FIG. 3 - DETAILS OF TEST BEAMS

FIG. 4 - INSTRUMENTATION OF BEAMS

FIG. 5 - HOLE EDGE STRESSES (HOLE 1, BEAM A)

FIG. 6 - HOLE EDGE STRESSES (HOLE 2, BEAM A)

FIG. 7 - HOLE EDGE STRESSES (HOLE 3, BEAM B)

FIG. 8 - HOLE EDGE STRESSES (HOLE 4, BEAM B)

FIG. 9 - SHEAR STRESSES AT HOLE CENTRELINE (HOLE 3, BEAM B)

FIG. 10 - SHEAR STRESSES AT HOLE CENTRELINE (HOLE 4, BEAM B)

FIG. 11 - FLANGE STRESSES (HOLE 2, BEAM A)

FIG. 12 - FLANGE STRESSES (HOLE 3, BEAM B)

FIG. 13 - SHEAR STRESSES AT HOLE CENTRELINE (REF. 5)

FIG. 14 - COMPARISON OF ANALYTICAL METHODS

FIG. 15 - GOVERNING STRESSES ON INTERACTION DIAGRAM

FIG. 16 - DESIGN CURVE (2R/d = 0.20)

FIG. 17 - DESIGN CURVE (2R/d = 0.25)

FIG. 18 - DESIGN CURVE (2R/d = 0.30)

FIG. 19 - DESIGN CURVE (2R/d = 0.35)

FIG. 20 - DESIGN CURVE (2R/d = 0.40)

FIG. 21 - DESIGN CURVE (2R/d = 0.45)

FIG. 22 - DESIGN CURVE (2R/d = 0.50)

FIG. 23 - DESIGN CURVE (2R/d = 0.55)

FIG. 24 - DESIGN CURVE (2R/d = 0.60)

FIG. 25 - DESIGN CURVE (2R/d = 0.65)

FIG. 26 - DESIGN CURVE (2R/d = 0.70)

FIG. 27 - DESIGN CURVE (2R/d = 0.75)

FIG. 28 - DIVISION OF SHEAR FORCE

FIG. 29 - EXAMPLE

FIG. 30 - FREE-BODY DIAGRAM FOR SHEAR DIVISION

FIG. 31 - TYPICAL VERTICAL TEE-SECTION

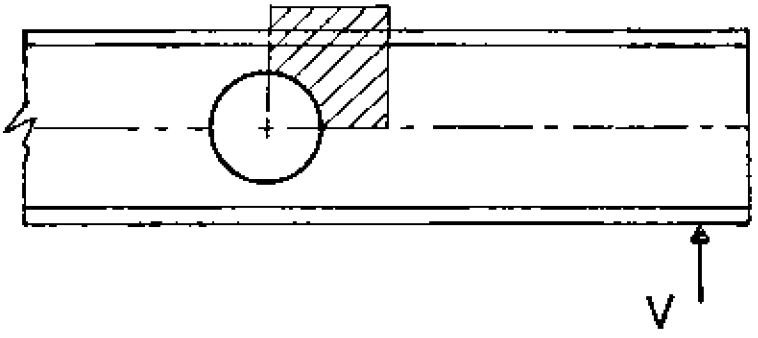
V

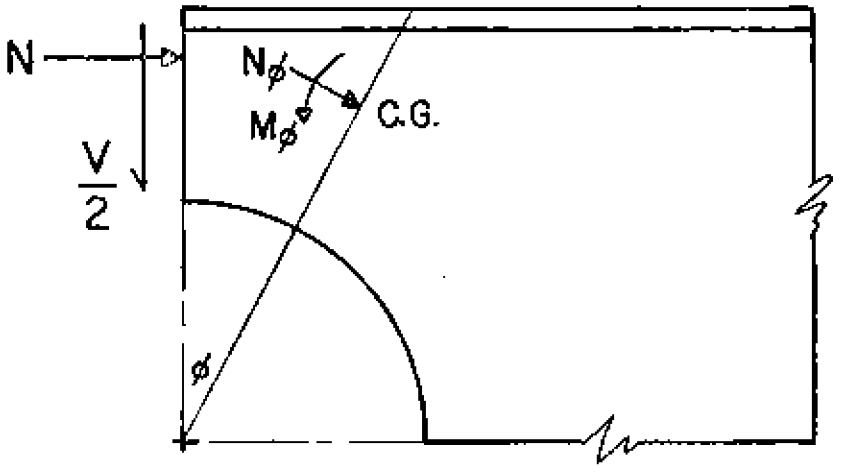
N
V/2
Nϕ
Mϕ
C.G.
ϕ

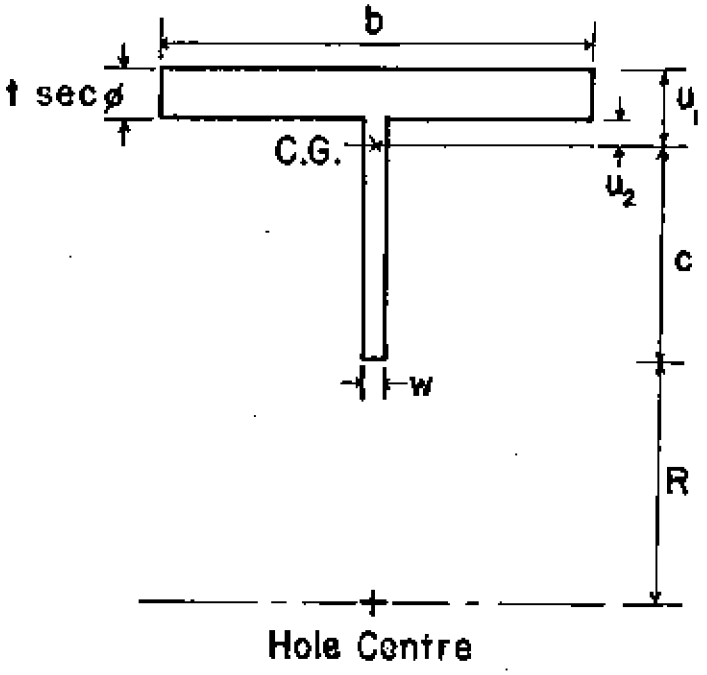
b
t sec ø
C.G.
u_1
u_2
c
w
R
Hole Centre

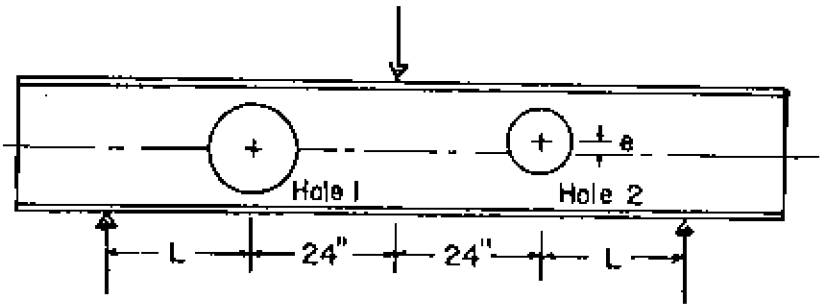

BEAM A
W14×30

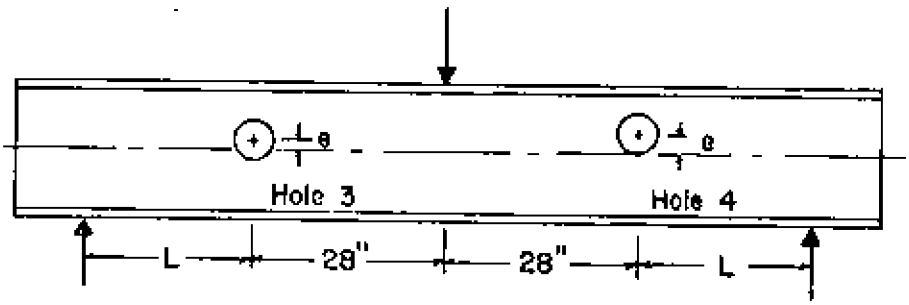

BEAM B
W14×38

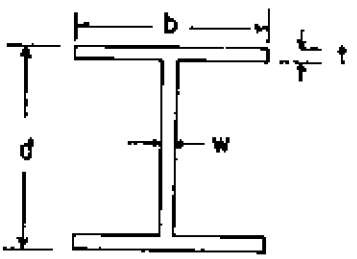

Beam	d	b	t	w	Hole	Dia. (2R) (in.)	e (in.)	$\frac{2R}{d}$	e/d	L (in.) Test 1	L (in.) Test 2
A	14.0	6.75	.38	.27	1	10.5	0	.750	0	48	24
					2	8.0	1.25	.571	.089	48	24
B	14.2	6.75	.51	.32	3	5.0	1.00	.352	.070	48	24
					4	5.0	2.50	.352	.176	48	24

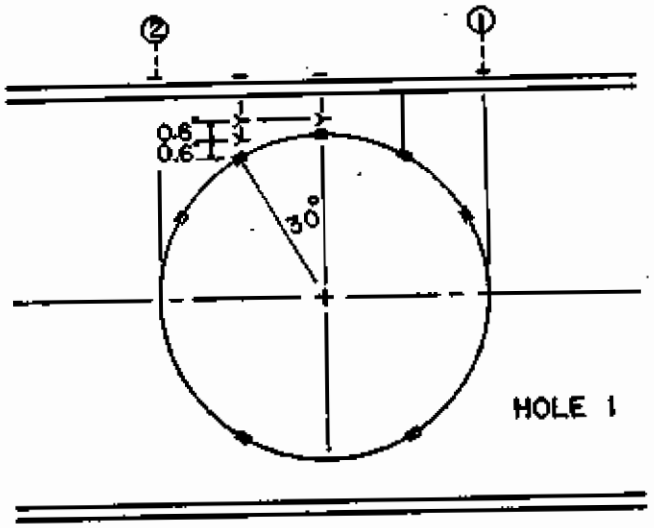

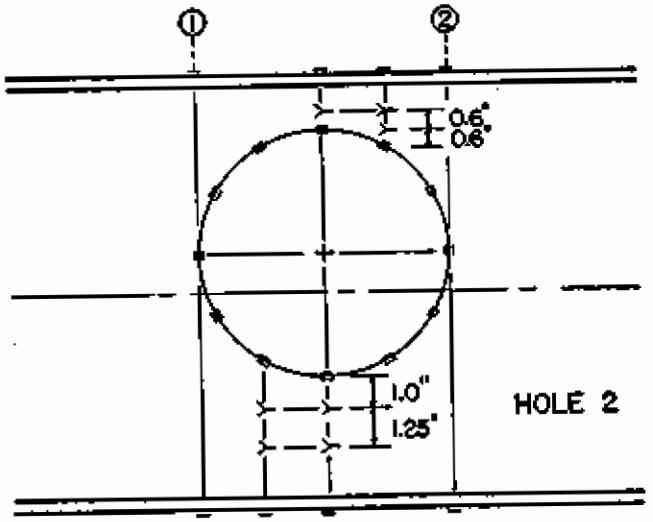

① HIGH MOMENT EDGE

② LOW MOMENT EDGE

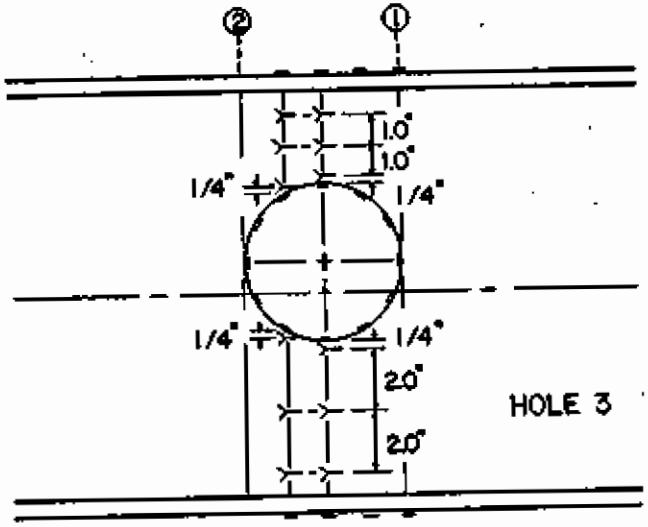

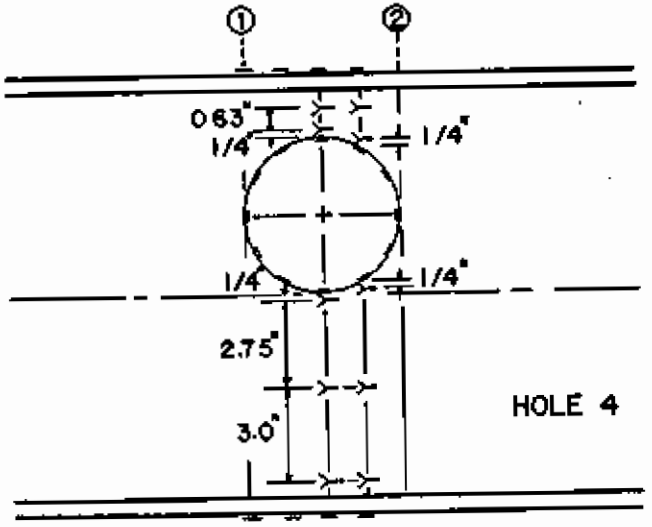

Fig 4.

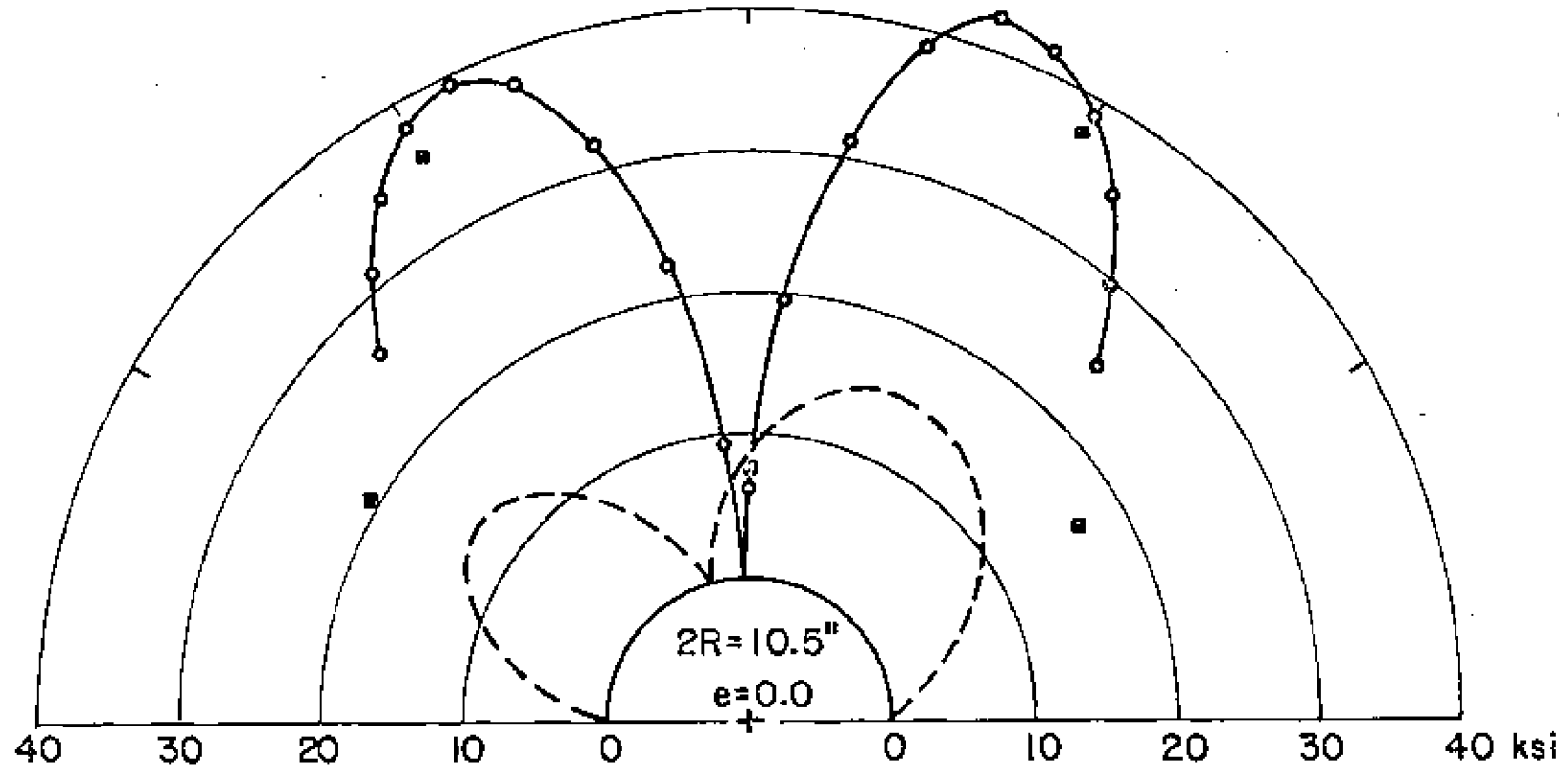

----ELASTICITY

—o— CURVED BEAM

▪ EXPERIMENT

BEAM A

HOLE 1

M = 240 kip in

V = 10 kips

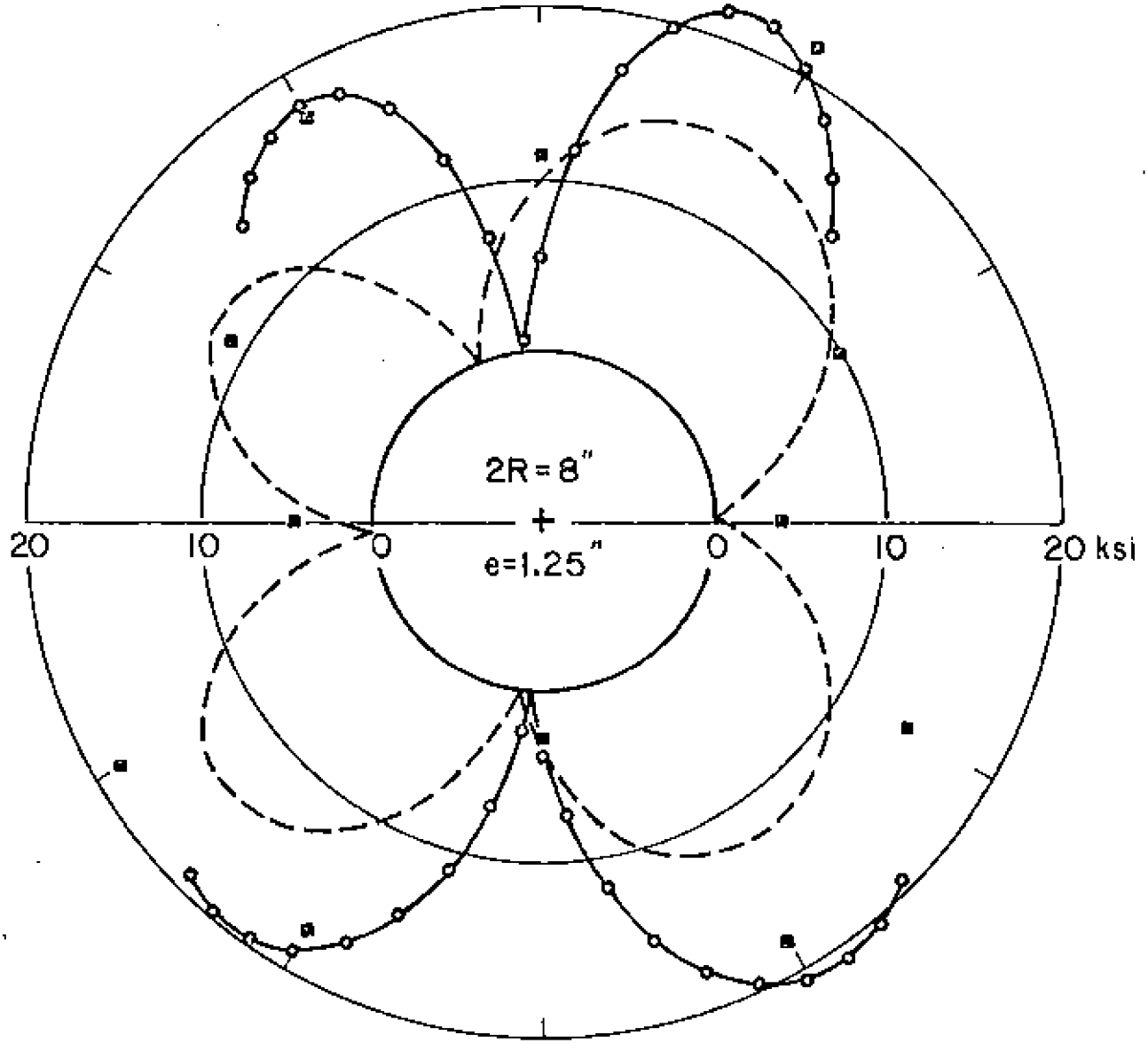

---- ELASTICITY

—o— CURVED BEAM

■ EXPERIMENT

BEAM A

HOLE 2

M=240-kip in

V=10 kips

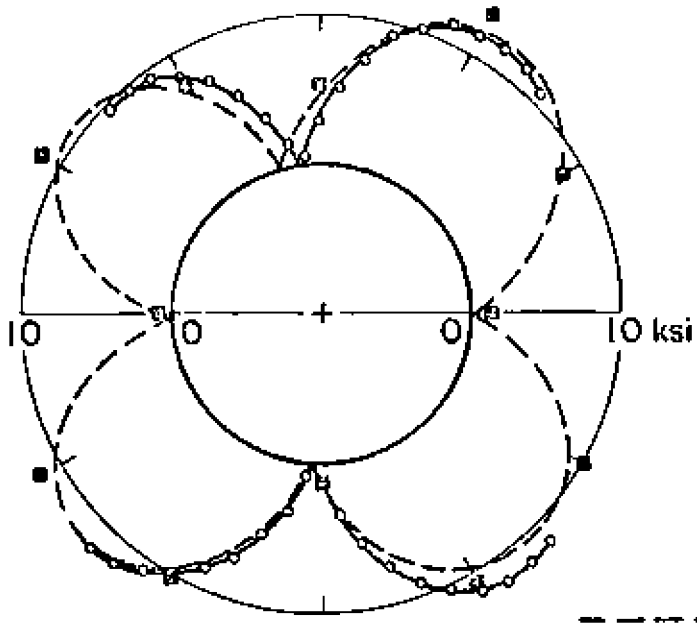

M = 240 kip in
V = 10 kips

– – – – ELASTICITY
—o— CURVED BEAM
■ EXPERIMENT

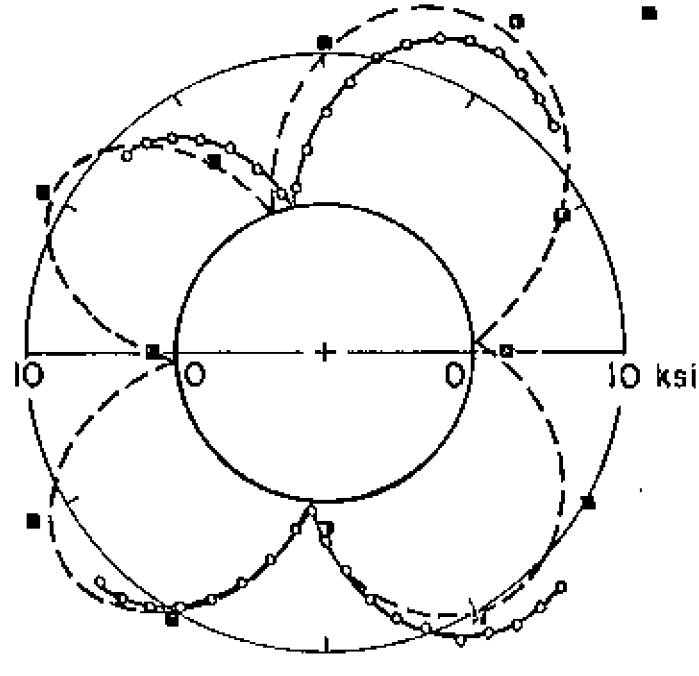

M = 480 kip in
V = 10 kips

BEAM B
HOLE 3

2R = 5"
e = 1.0"

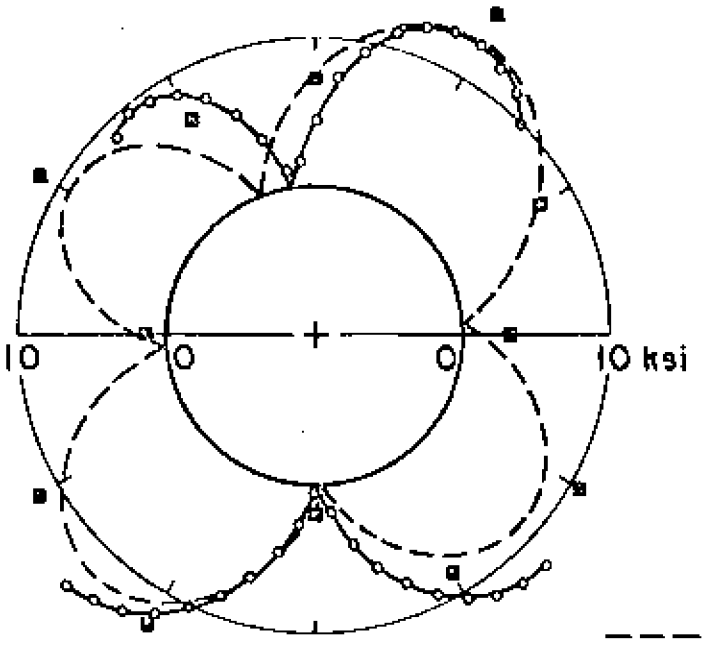

M=240 kip in
V=10 kips

----ELASTICITY
—o—CURVED BEAM
■ EXPERIMENT

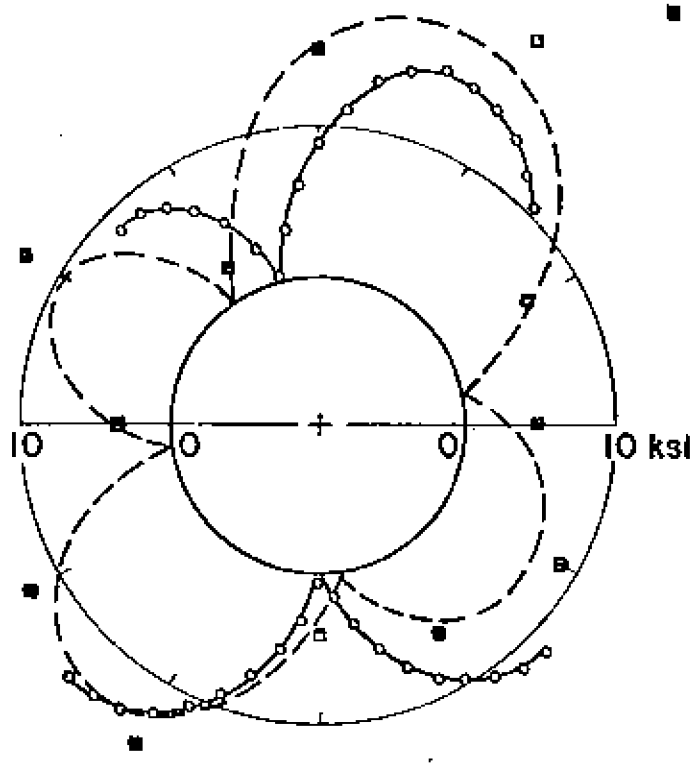

M=480 kip-in
V=10 kips

BEAM B
HOLE 4

2R = 5"
e = 2.5"

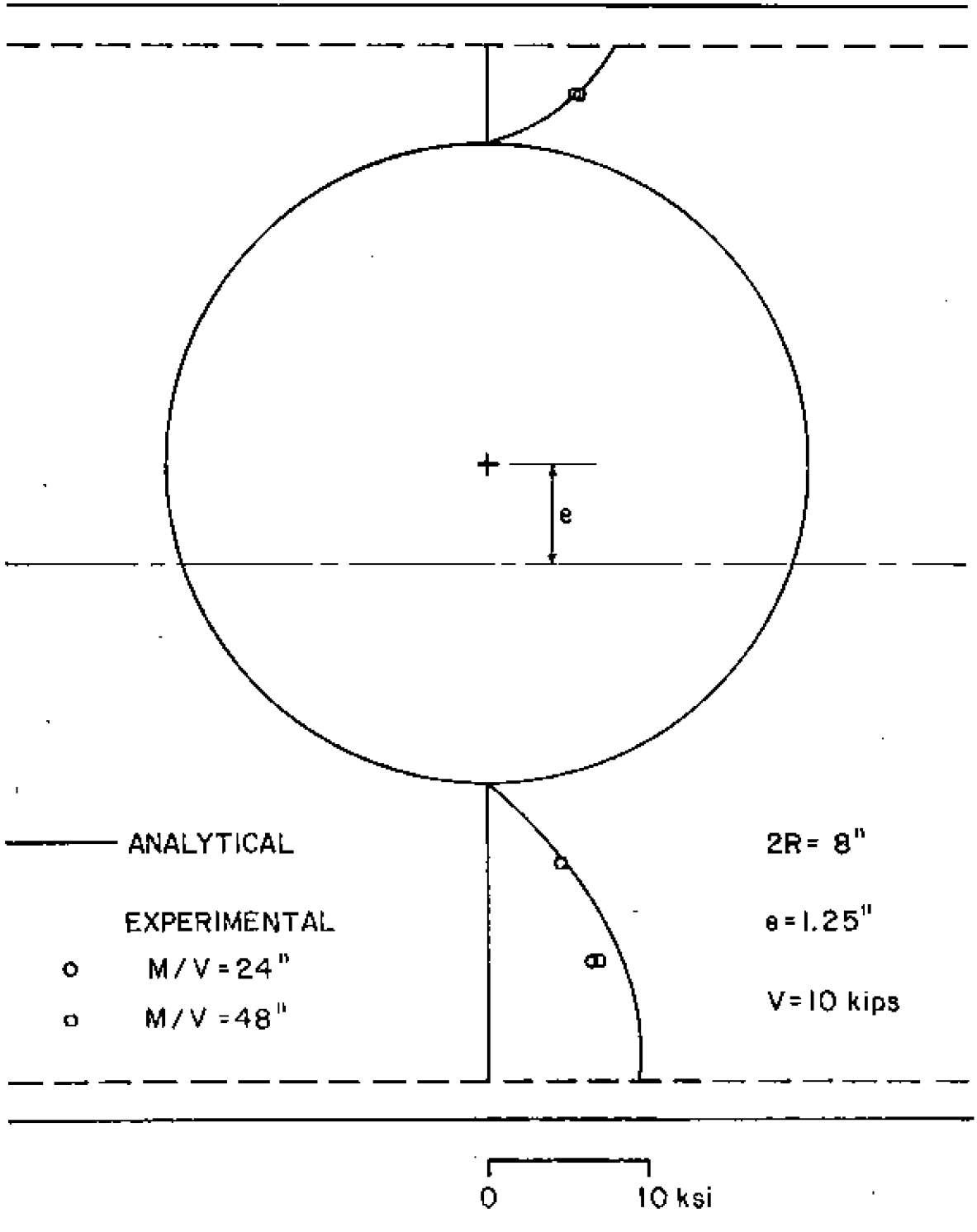
e
ANALYTICAL
EXPERIMENTAL
M/V = 24"
M/V = 48"
2R = 8"
e = 1.25"
V = 10 kips
0
10 ksi

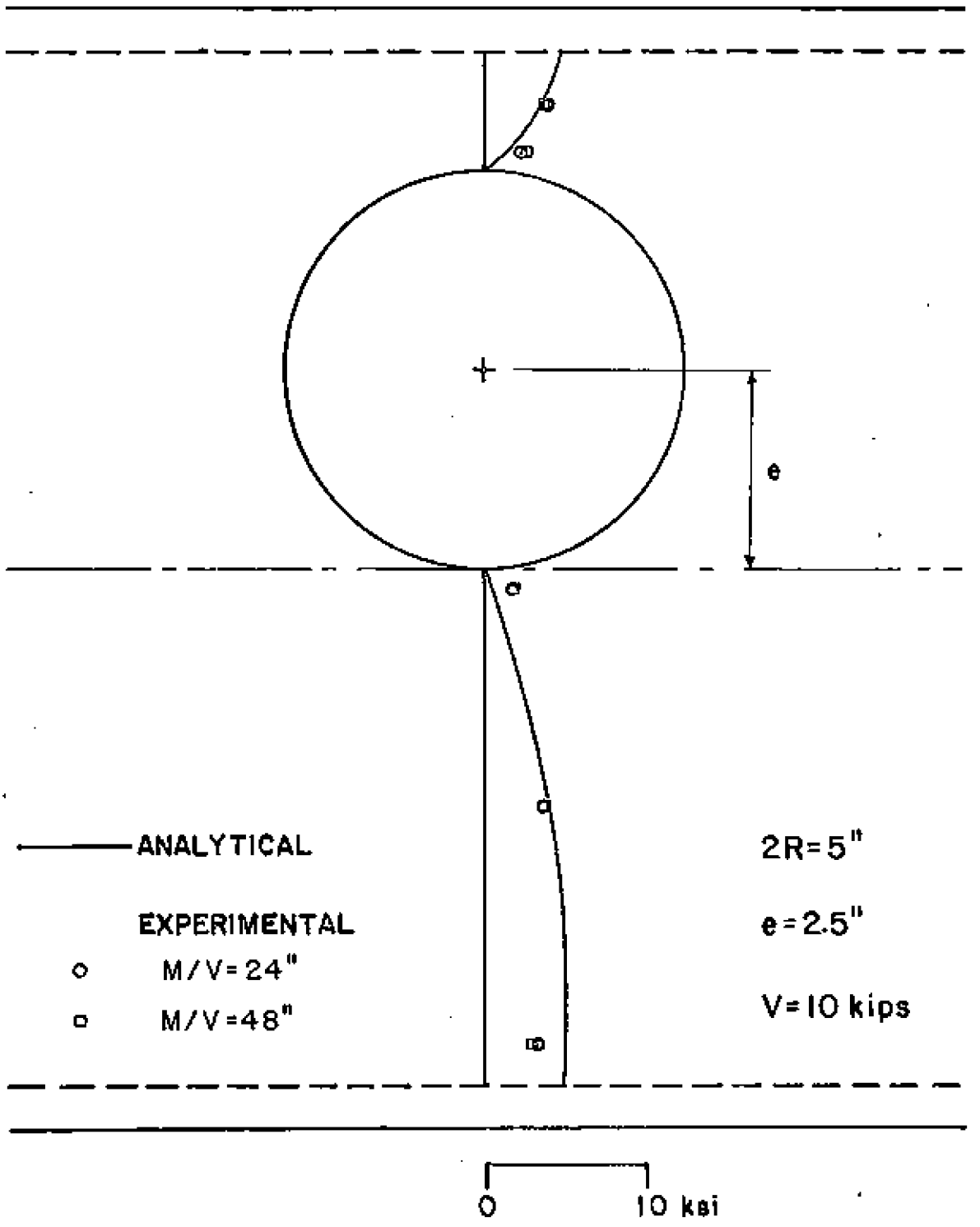
e
ANALYTICAL
EXPERIMENTAL
M/V=24"
M/V=48"
2R=5"
e=2.5"
V=10 kips
0
10 ksi

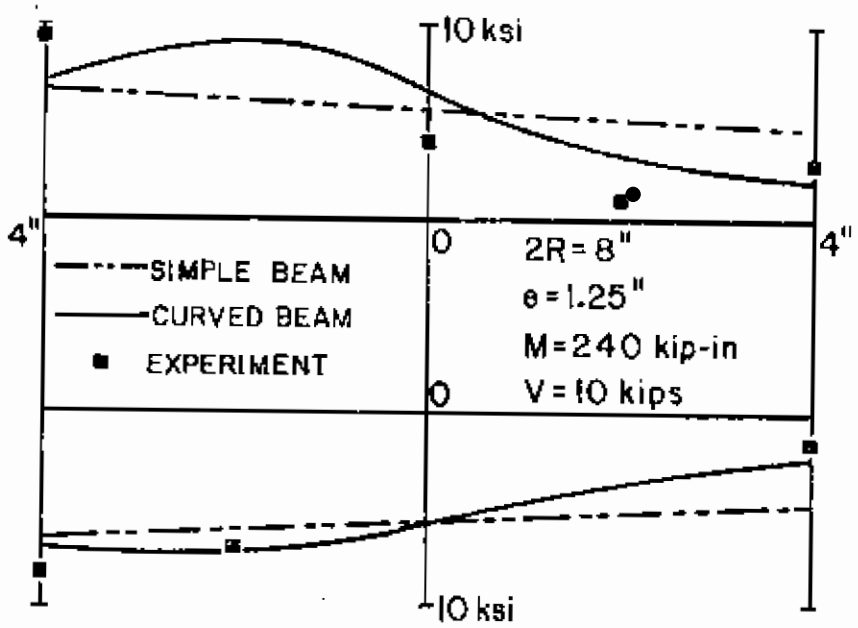
10 ksi
4"
4"
0
0
SIMPLE BEAM
CURVED BEAM
EXPERIMENT
2R = 8"
e = 1.25"
M = 240 kip-in
V = 10 kips
10 ksi

Fig 4

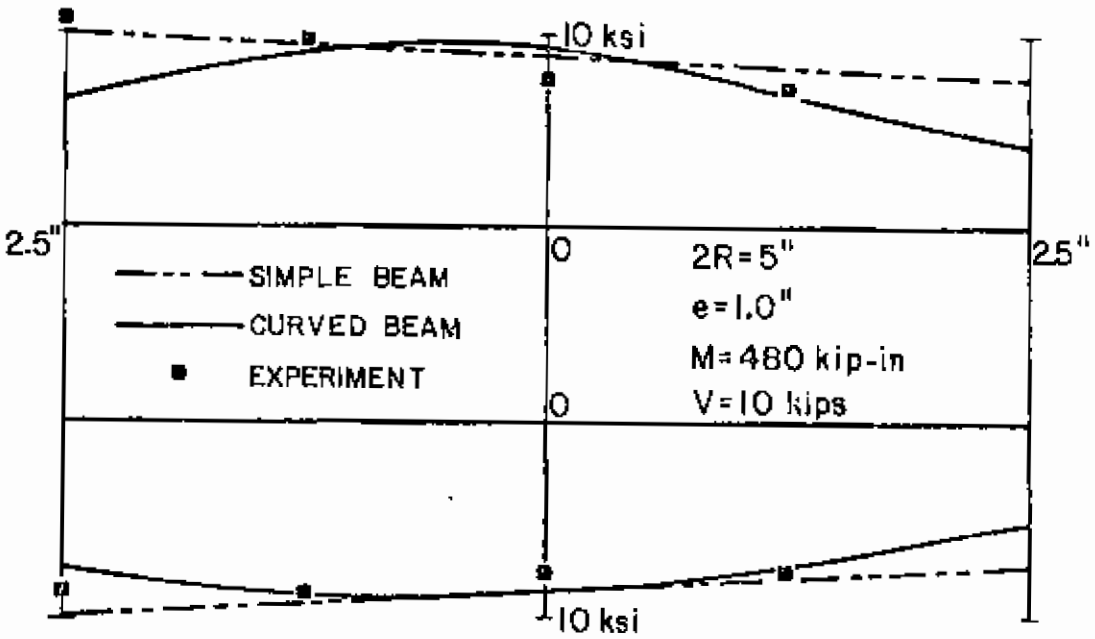
10 ksi
2.5"
2.5"
0
0
SIMPLE BEAM
CURVED BEAM
EXPERIMENT
2R = 5"
e = 1.0"
M = 480 kip-in
V = 10 kips
10 ksi

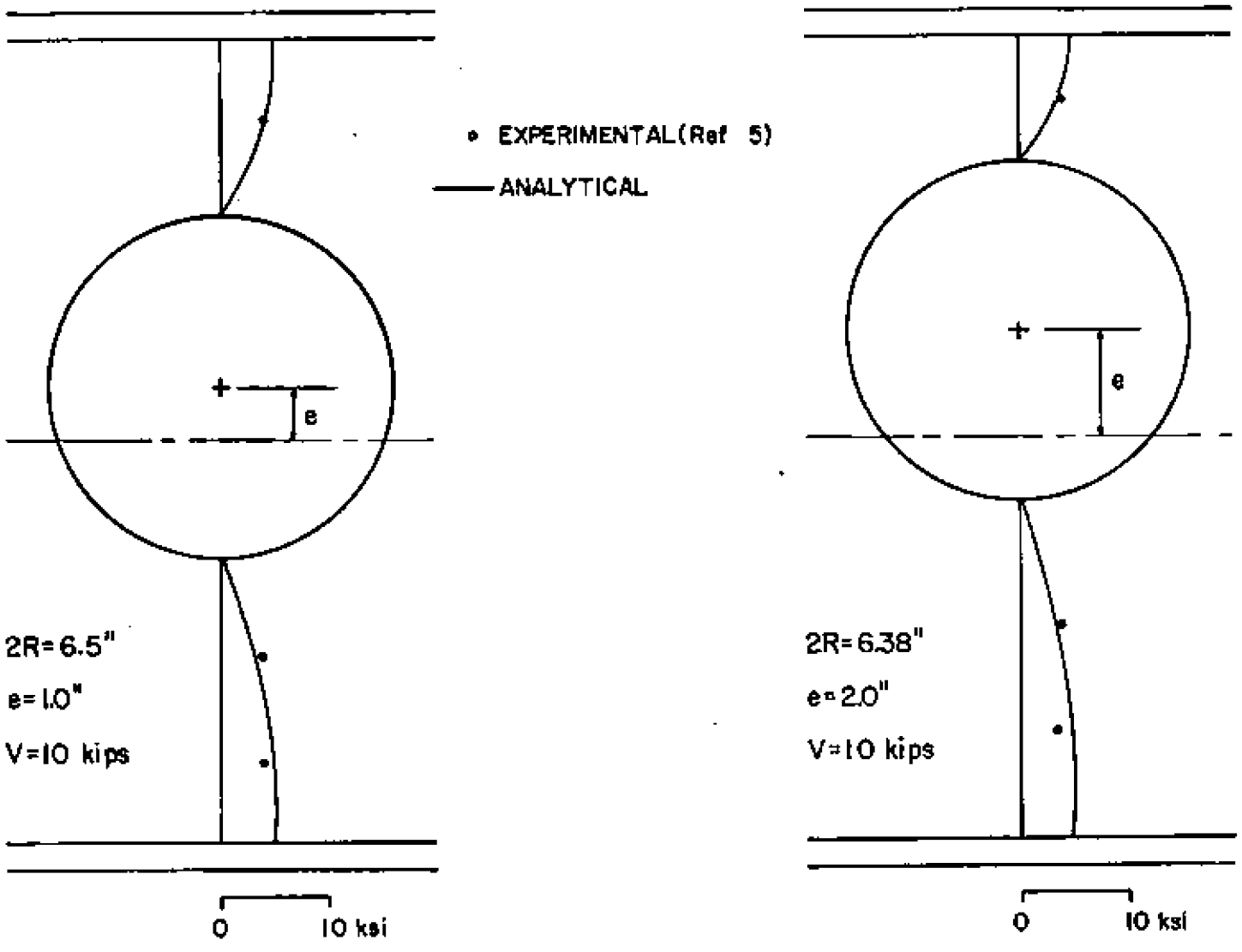
• EXPERIMENTAL(Ref 5)
ANALYTICAL
2R=6.5"
e=1.0"
V=10 kips
e
0
10 ksi
2R=6.38"
e=2.0"
V=10 kips
e
0
10 ksi

Fig 13

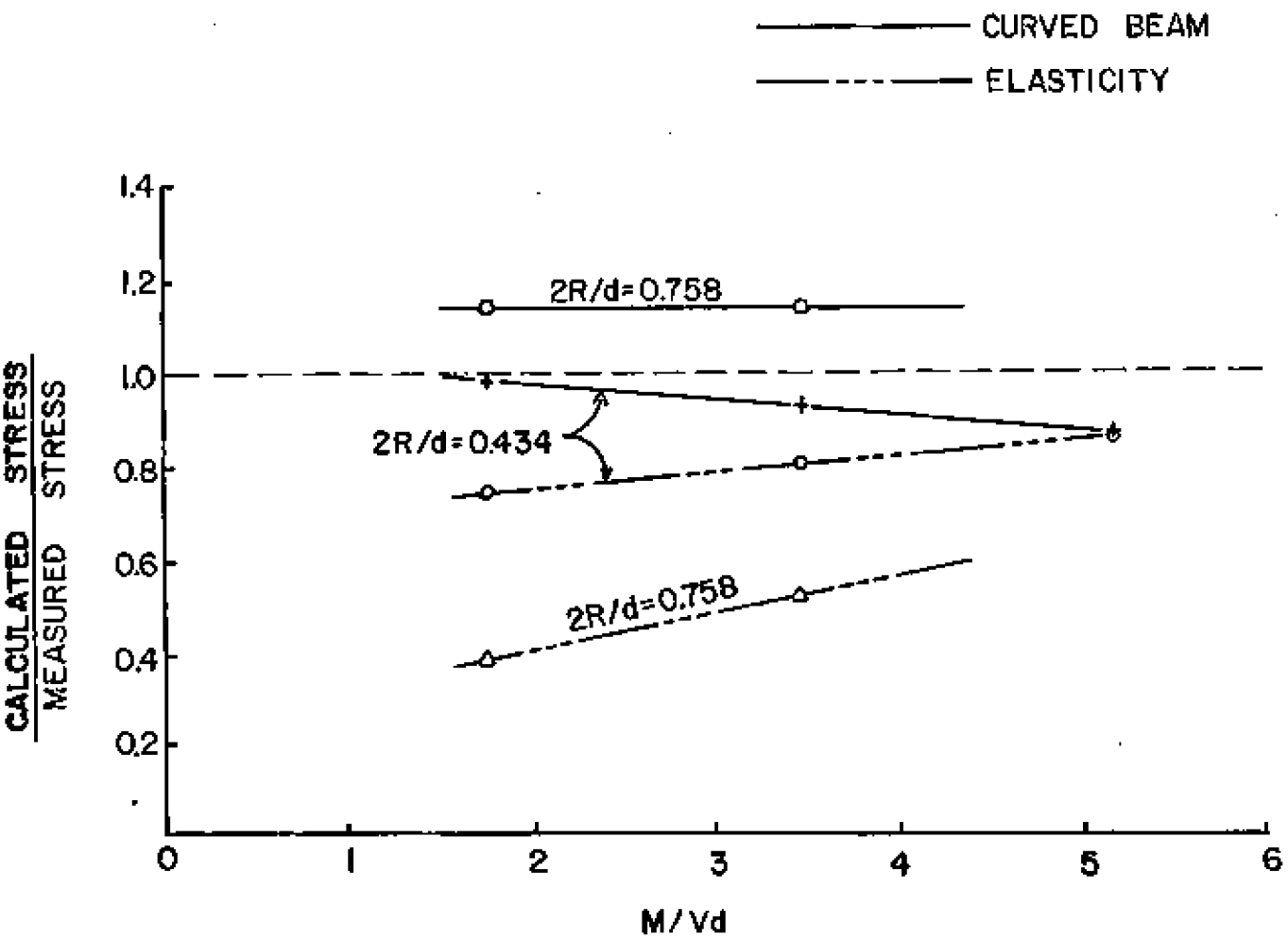
CURVED BEAM
ELASTICITY
1.4
1.2
1.0
0.8
0.6
0.4
0.2
0
1
2
3
4
5
6
2R/d=0.758
2R/d=0.434
2R/d=0.758
CALCULATED STRESS / MEASURED STRESS
M/Vd

Fig. 14

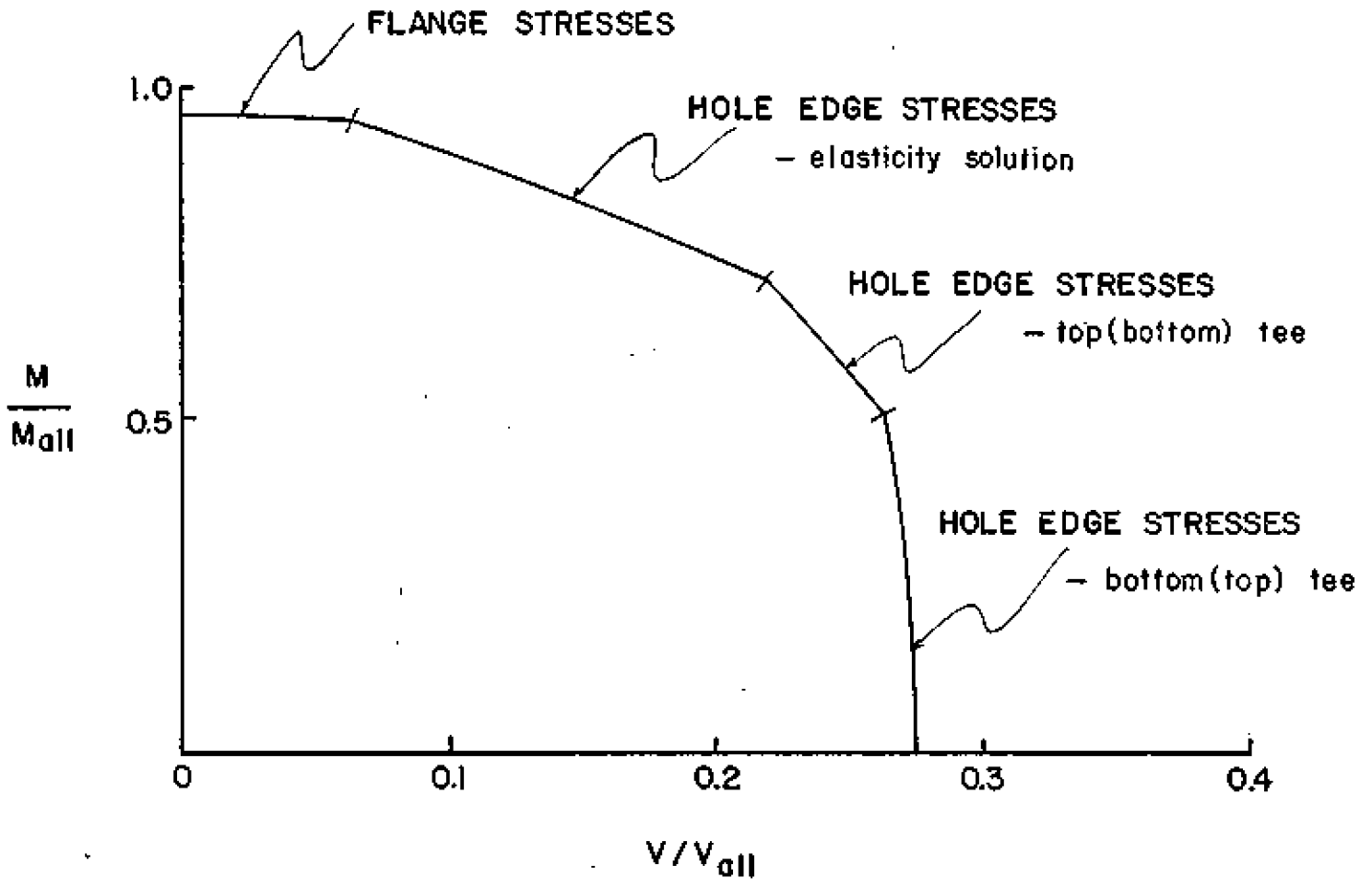
FLANGE STRESSES
HOLE EDGE STRESSES
– elasticity solution
HOLE EDGE STRESSES
– top(bottom) tee
HOLE EDGE STRESSES
– bottom(top) tee
1.0
0.5
M / Mall
0
0.1
0.2
0.3
0.4
V/Vall

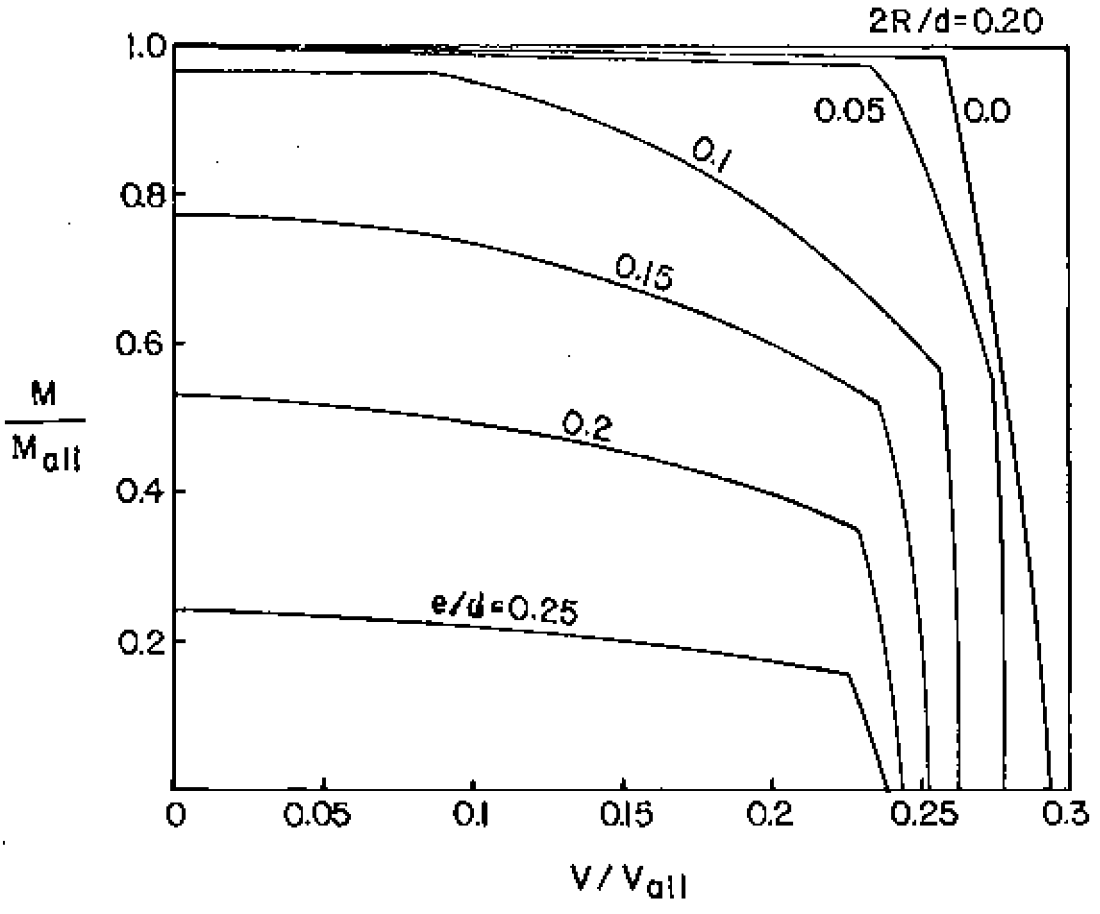
2R/d=0.20
1.0
0.8
0.6
0.4
0.2
M / M all
0.05
0.0
0.1
0.15
0.2
e/d=0.25
0
0.05
0.1
0.15
0.2
0.25
0.3
V / V all

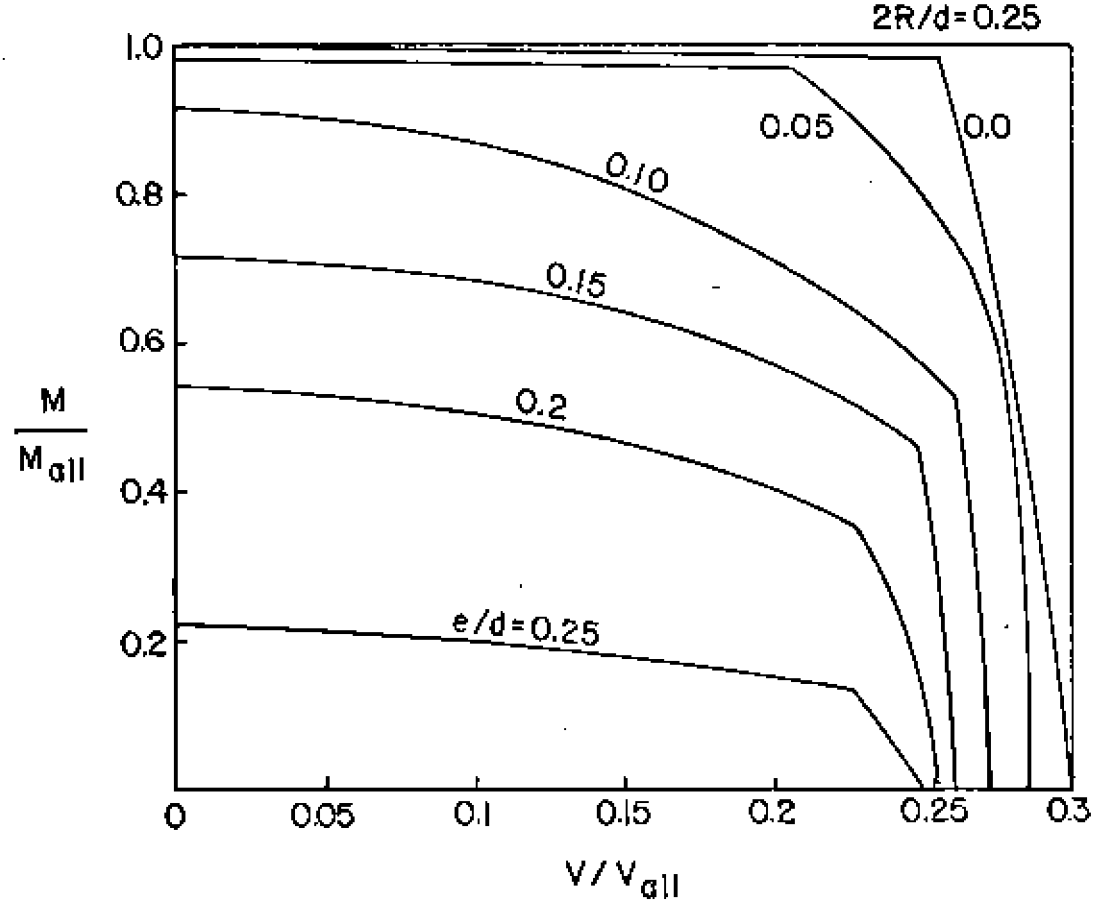
2R/d=0.25
1.0
0.8
0.6
0.4
0.2
M / M all
0.05
0.0
0.10
0.15
0.2
e/d=0.25
0
0.05
0.1
0.15
0.2
0.25
0.3
V / V all

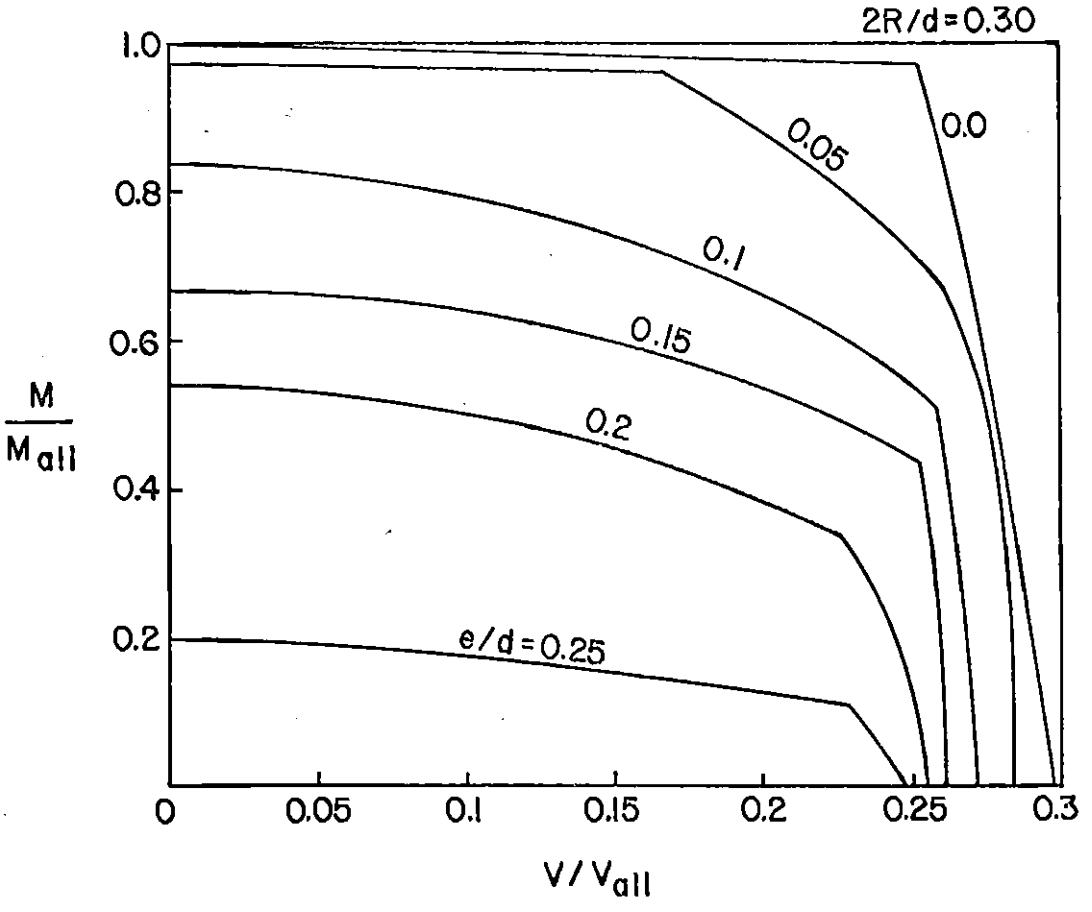
2R/d=0.30
1.0
0.8
0.6
0.4
0.2
M / Mall
0.0
0.05
0.1
0.15
0.2
e/d=0.25
0
0.05
0.1
0.15
0.2
0.25
0.3
V / Vall

Fig 18

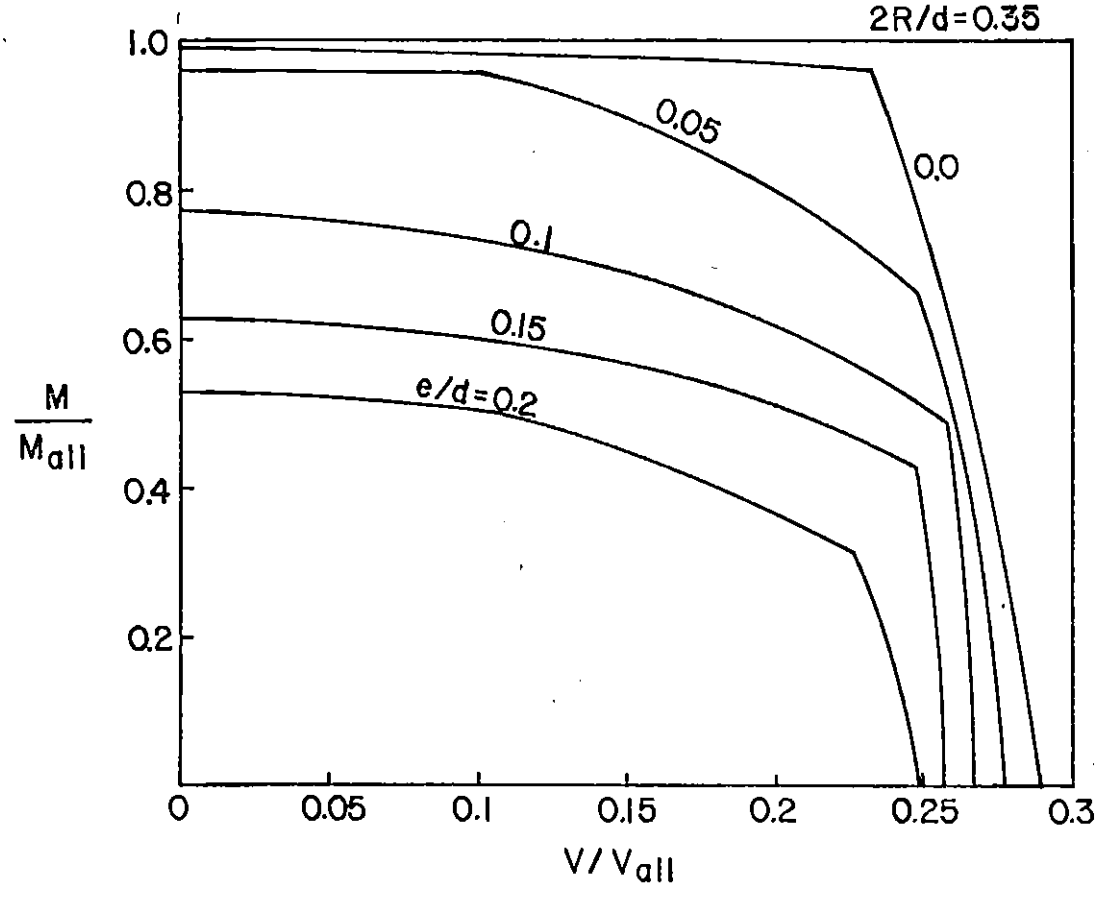
2R/d=0.35
1.0
0.8
0.6
0.4
0.2
M / Mall
0.0
0.05
0.1
0.15
e/d=0.2
0
0.05
0.1
0.15
0.2
0.25
0.3
V / Vall

Fig 19

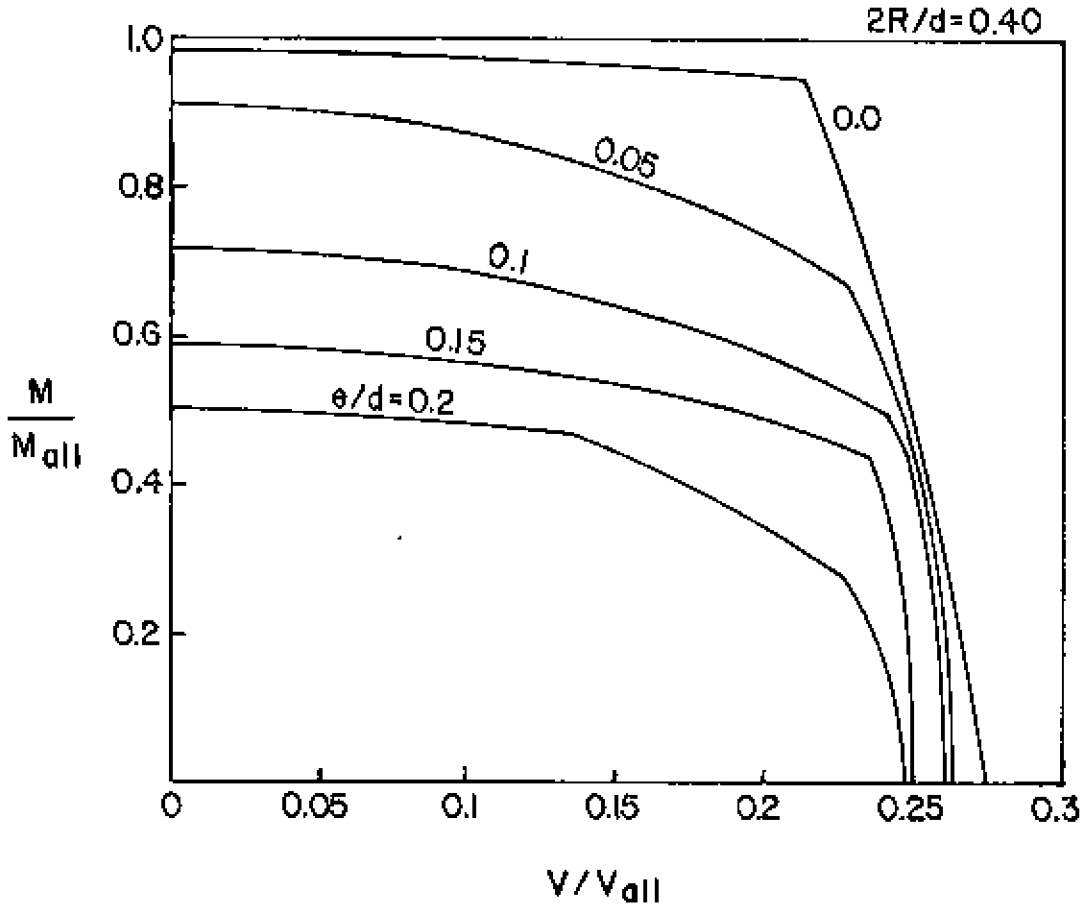
2R/d=0.40
1.0
0.8
0.6
0.4
0.2
0.0
0.05
0.1
0.15
e/d=0.2
M / Mall
0
0.05
0.1
0.15
0.2
0.25
0.3
V/Vall

Fig 2a

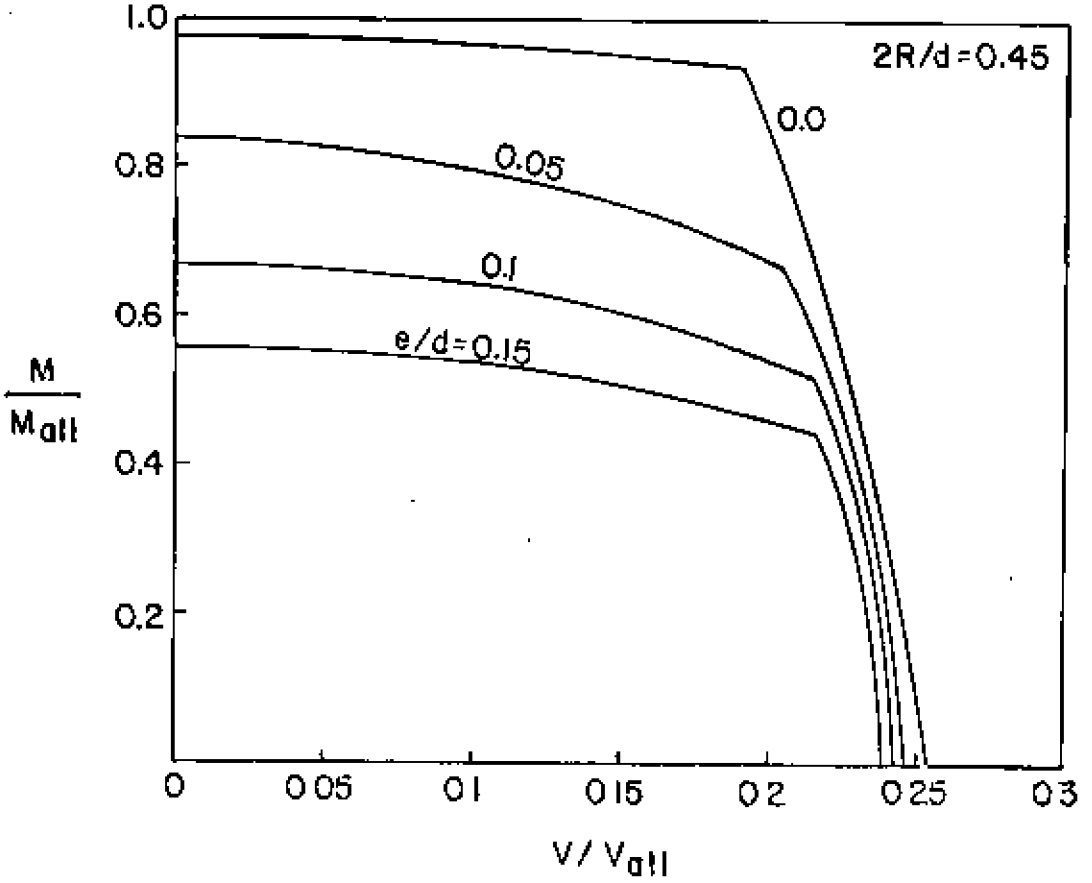
2R/d=0.45
1.0
0.8
0.6
0.4
0.2
0.0
0.05
0.1
e/d=0.15
M / Mall
0
0.05
0.1
0.15
0.2
0.25
0.3
V/Vall

Fig 2b

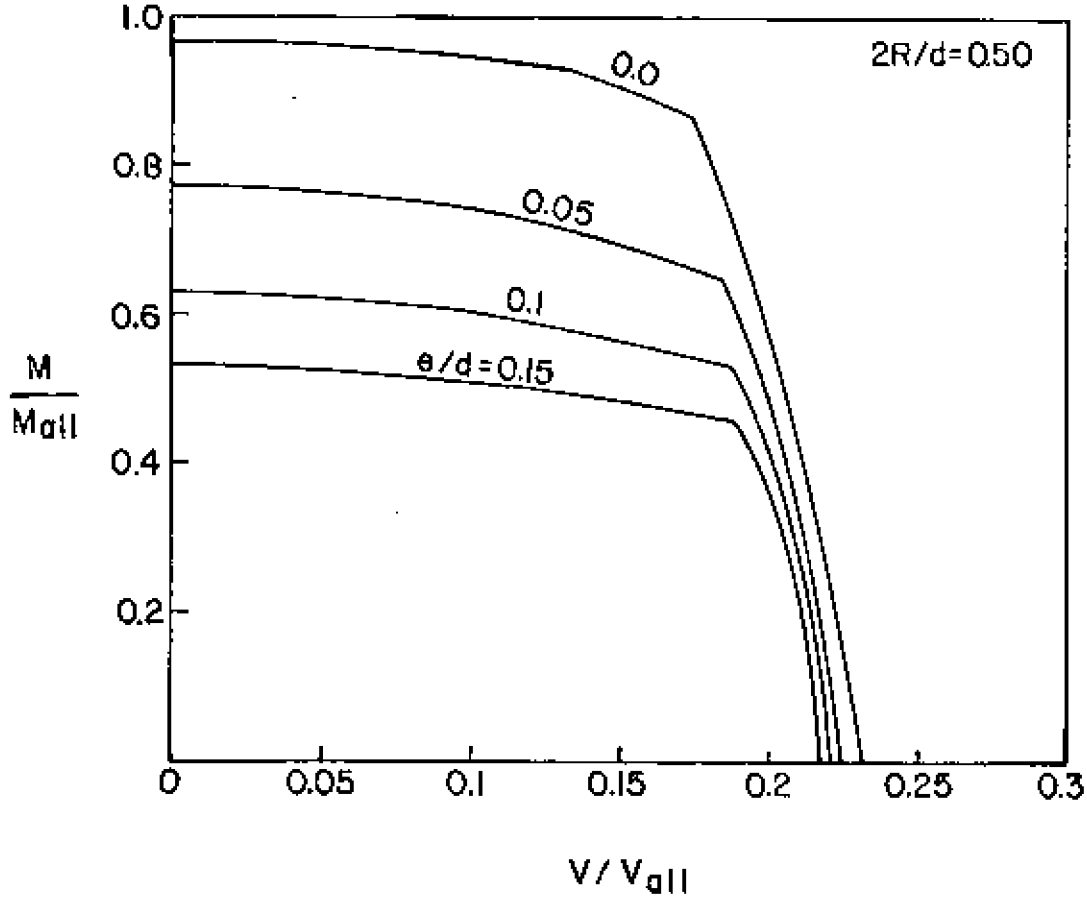
2R/d=0.50
0.0
0.05
0.1
e/d=0.15
M / Mall
V / Vall
1.0
0.8
0.6
0.4
0.2
0
0.05
0.1
0.15
0.2
0.25
0.3

Fig 2a

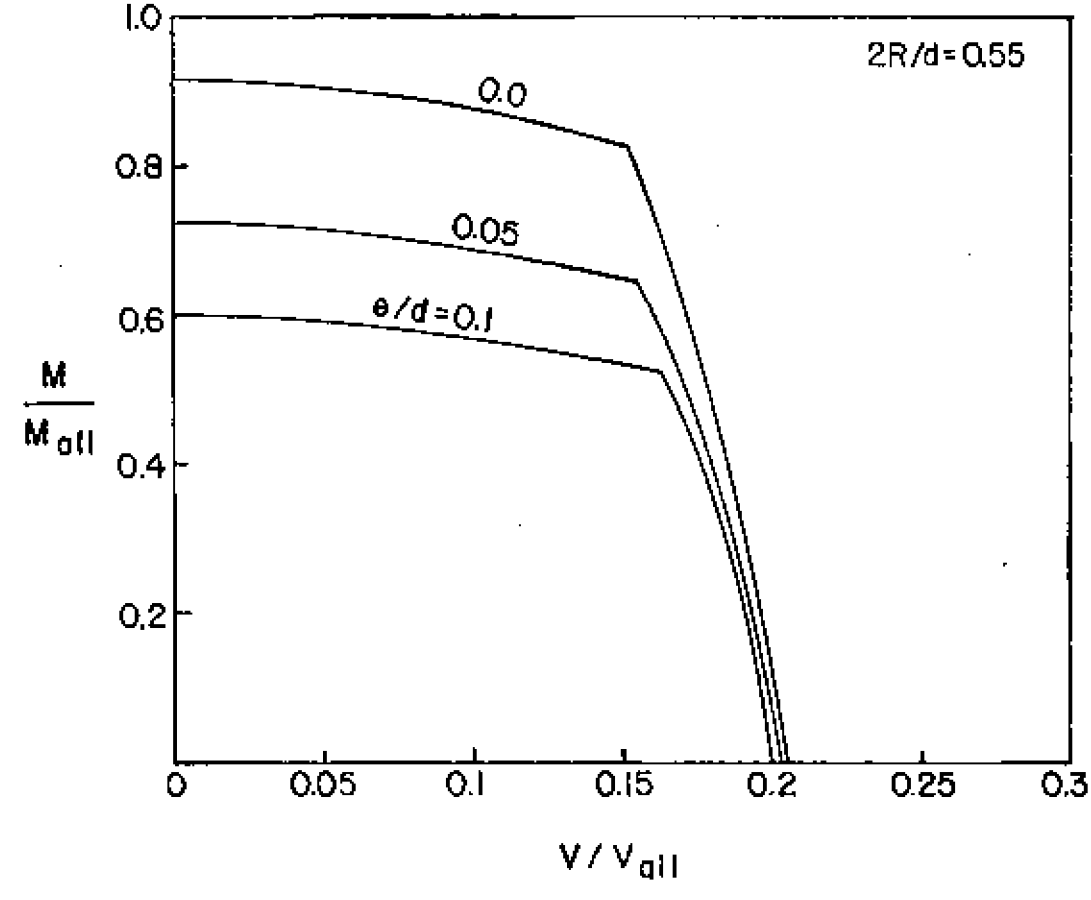
2R/d=0.55
0.0
0.05
e/d=0.1
M / Mall
V / Vall
1.0
0.8
0.6
0.4
0.2
0
0.05
0.1
0.15
0.2
0.25
0.3

Fig 2b

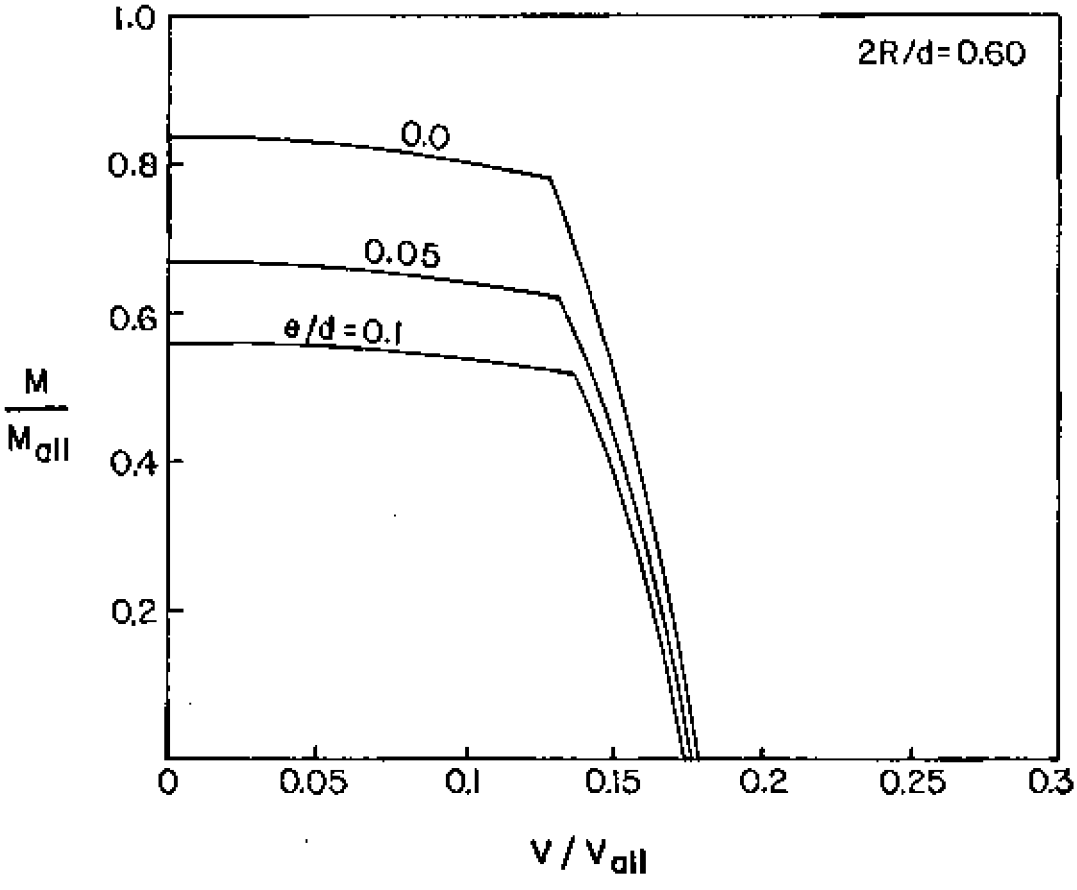
2R/d=0.60
0.0
0.05
e/d=0.1
M / Mall
V / Vall
1.0
0.8
0.6
0.4
0.2
0
0.05
0.1
0.15
0.2
0.25
0.3

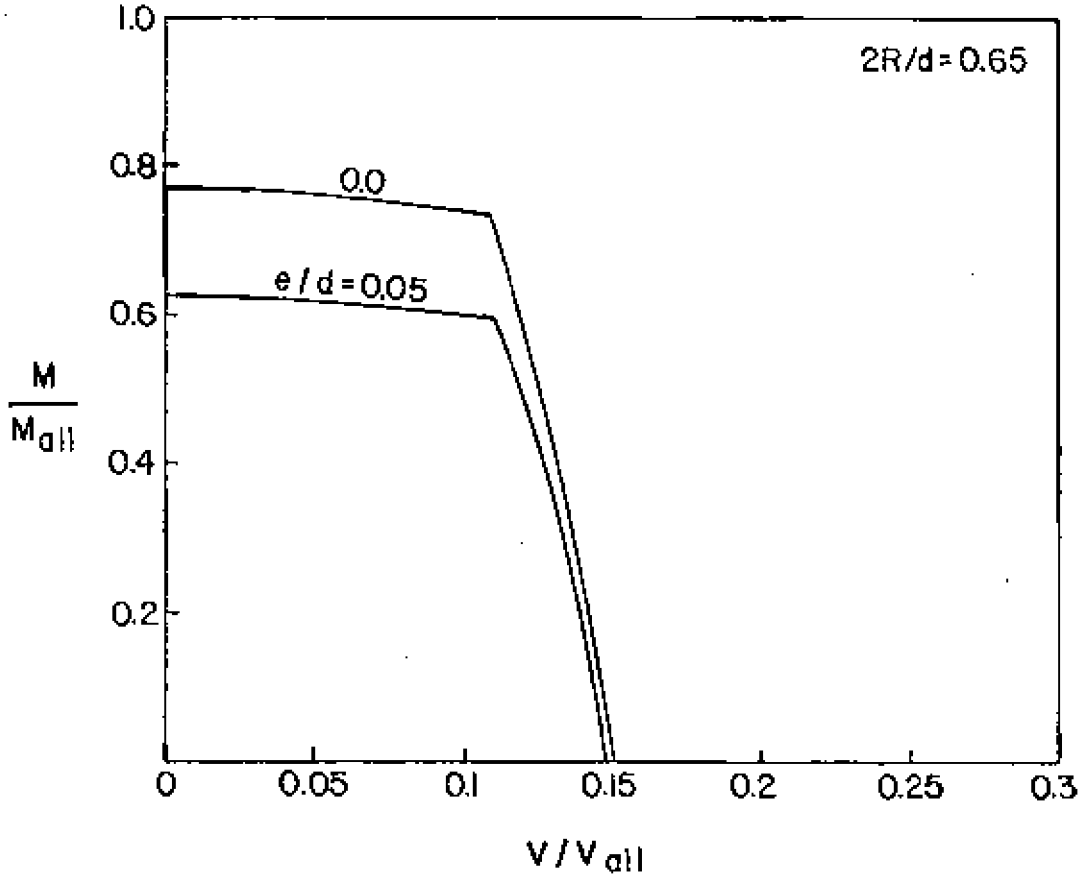
2R/d=0.65
0.0
e/d=0.05
M / Mall
V / Vall
1.0
0.8
0.6
0.4
0.2
0
0.05
0.1
0.15
0.2
0.25
0.3

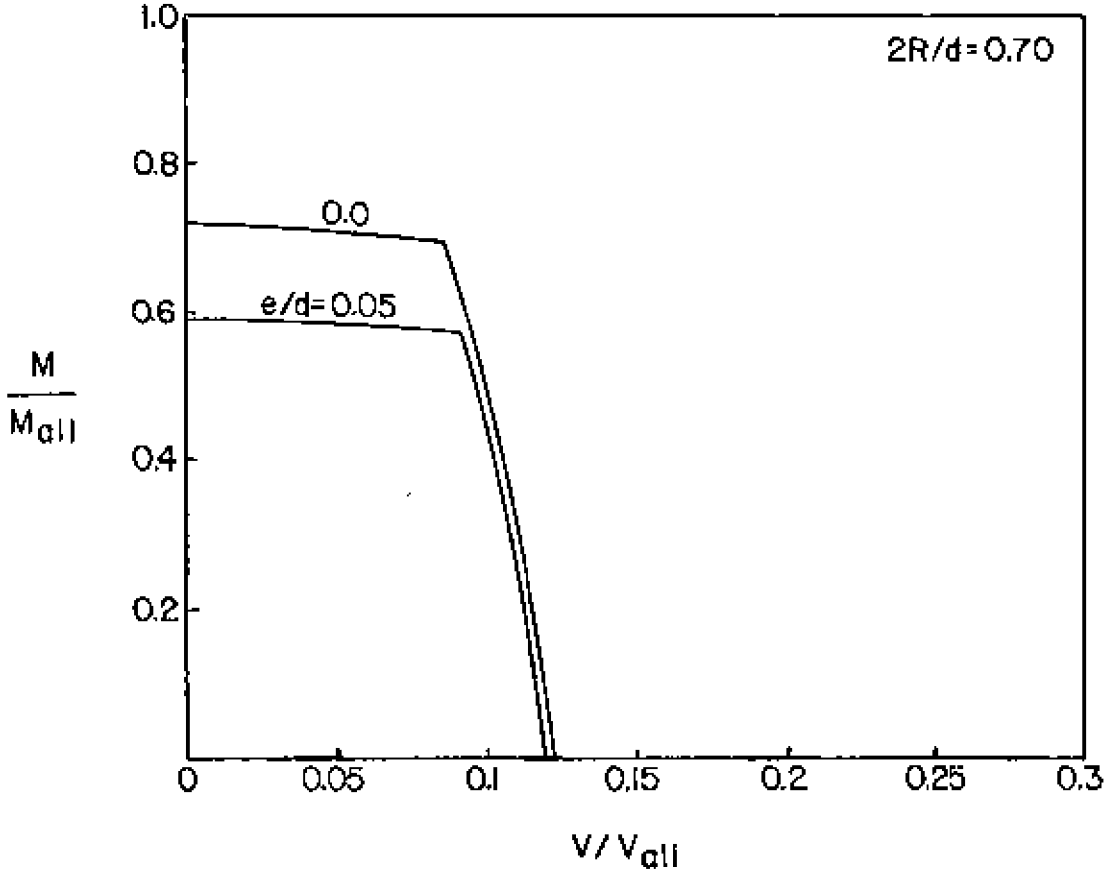
2R/d=0.70
0.0
e/d=0.05
M / M all
V / V all
1.0
0.8
0.6
0.4
0.2
0
0.05
0.1
0.15
0.2
0.25
0.3

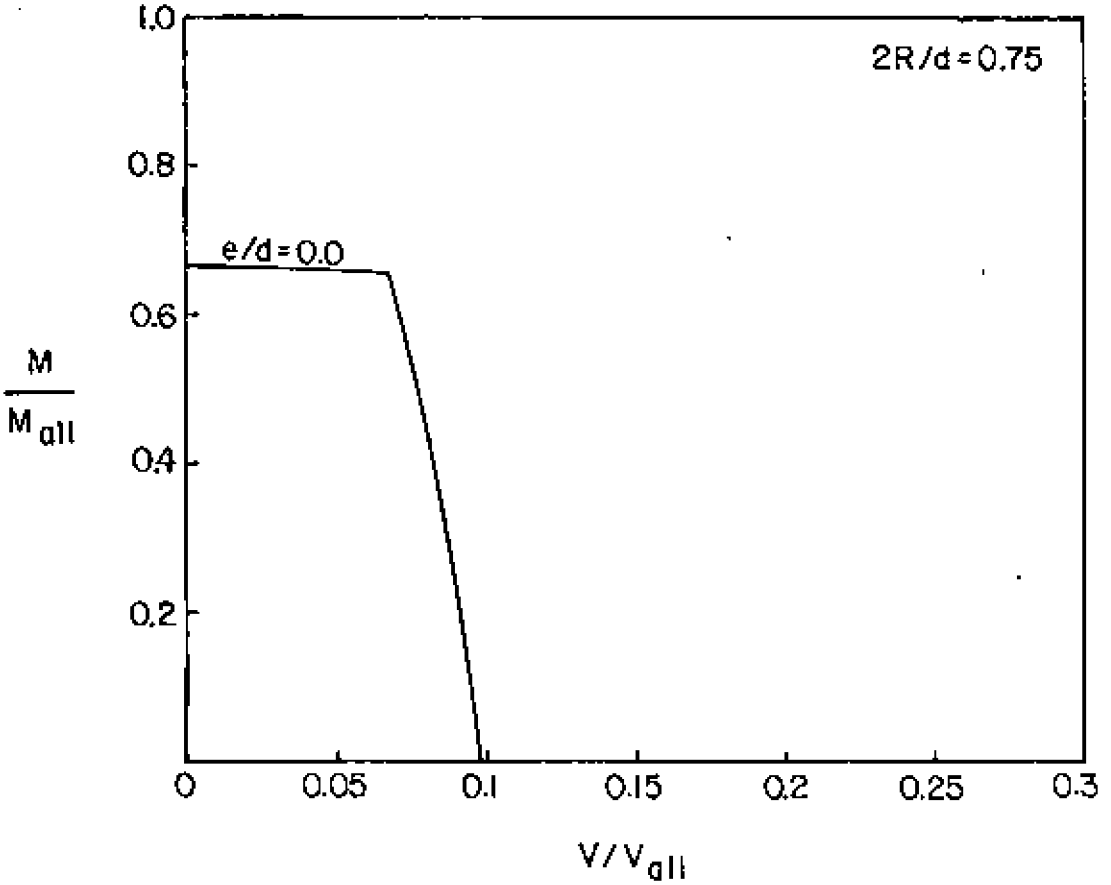
2R/d=0.75
e/d=0.0
M / M all
V / V all
1.0
0.8
0.6
0.4
0.2
0
0.05
0.1
0.15
0.2
0.25
0.3

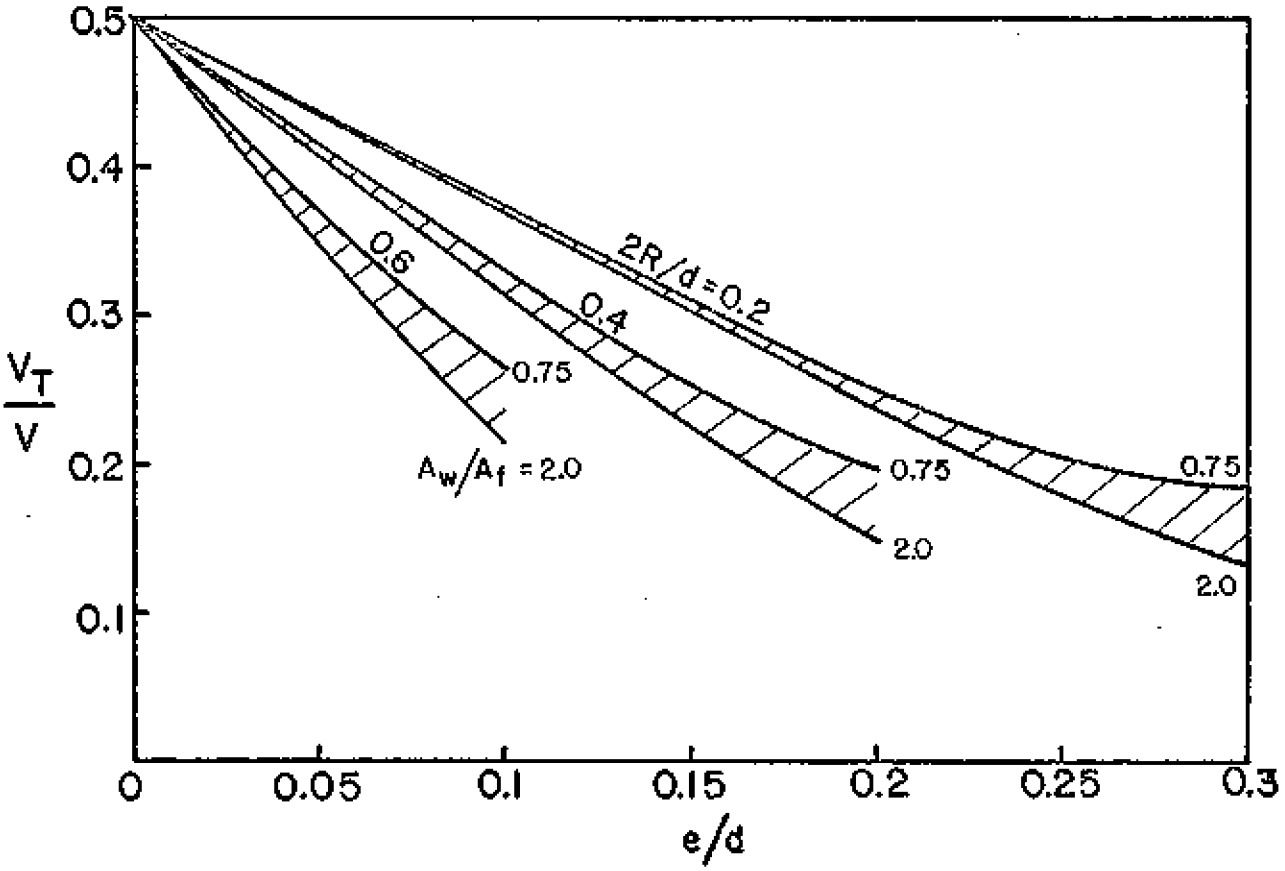
0.5
0.4
0.3
0.2
0.1
$\frac{V_T}{V}$
2R/d=0.2
0.6
0.4
0.75
A_w/A_f = 2.0
0.75
2.0
0.75
2.0
0
0.05
0.1
0.15
0.2
0.25
0.3
e/d

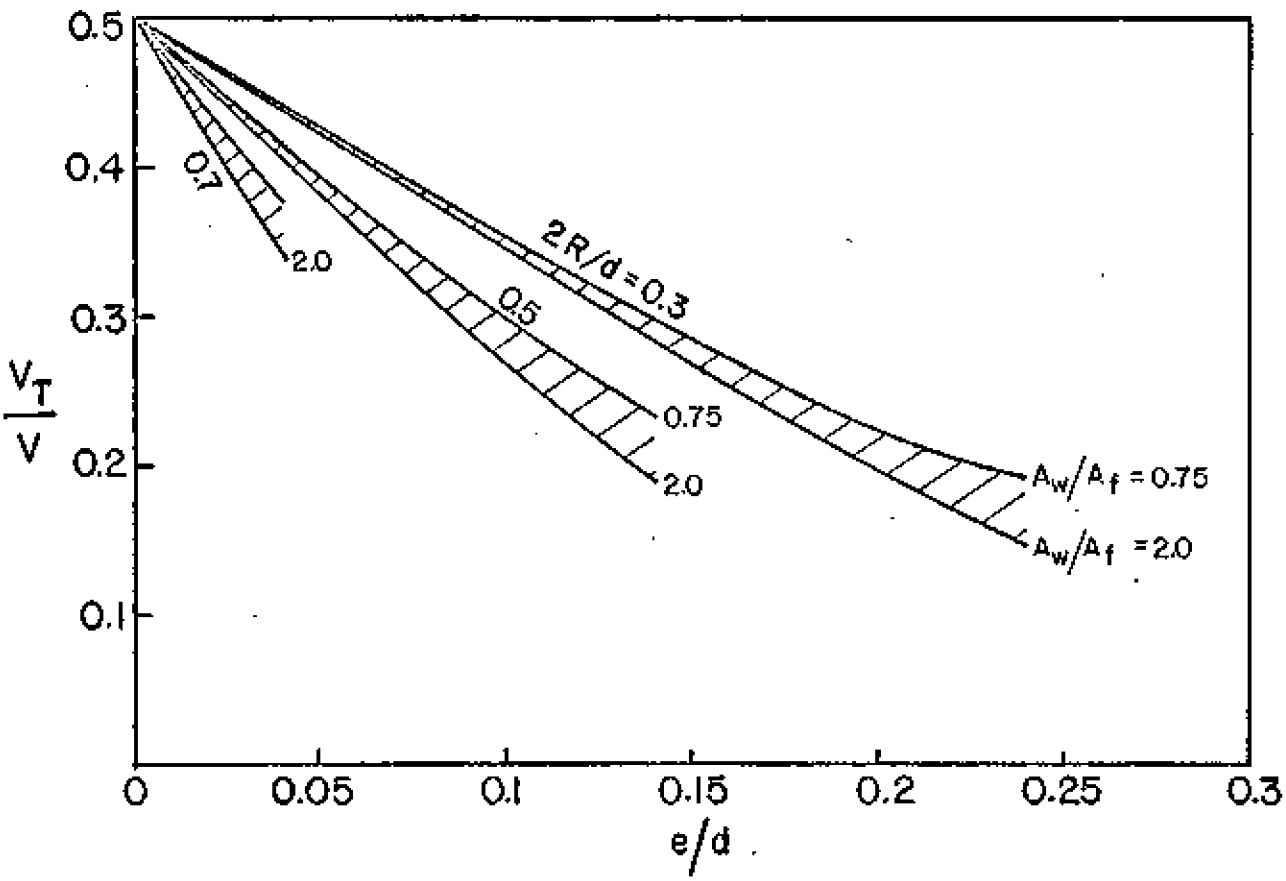
0.5
0.4
0.3
0.2
0.1
$\frac{V_T}{V}$
0.1
2.0
2R/d=0.3
0.5
0.75
2.0
A_w/A_f = 0.75
A_w/A_f = 2.0
0
0.05
0.1
0.15
0.2
0.25
0.3
e/d

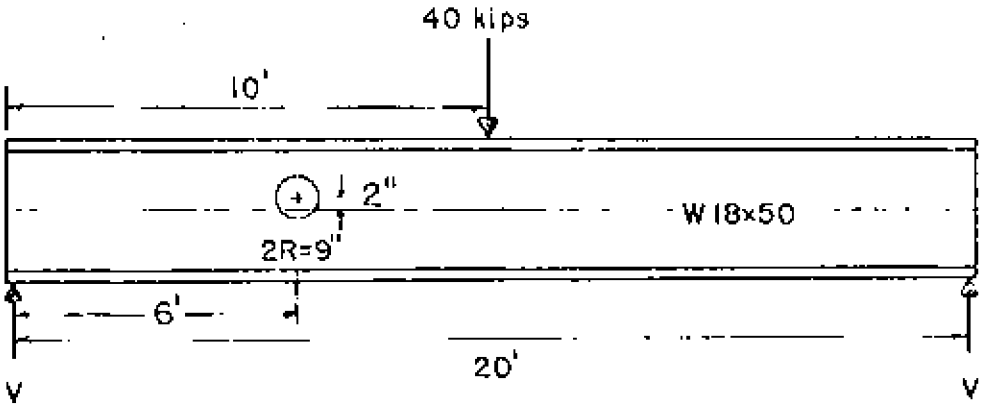
40 kips
10'
2"
W18×50
2R=9"
6'
20'
V
V

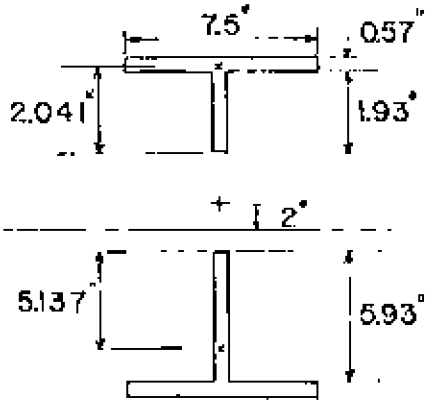
7.5"
0.57"
2.041"
1.93"
2"
5.137"
5.93"

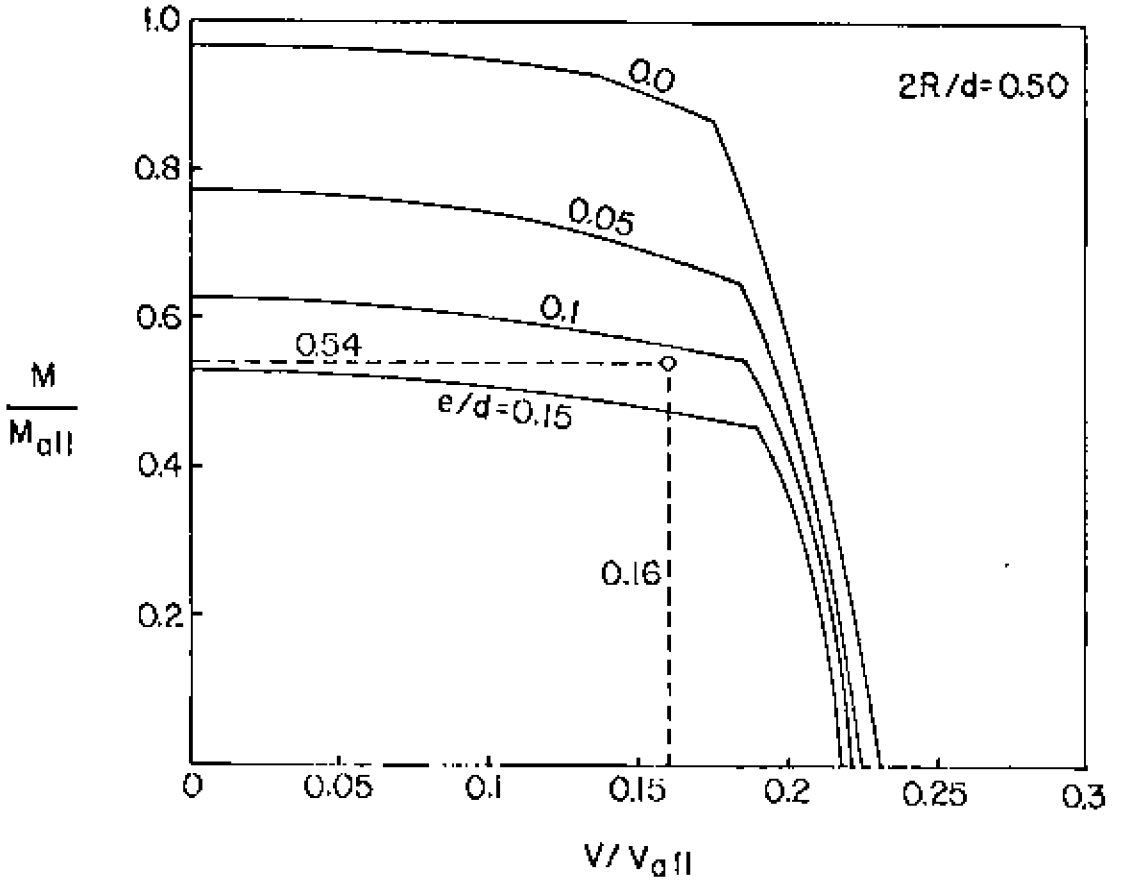
1.0
0.8
0.6
0.4
0.2
0
0.05
0.1
0.15
0.2
0.25
0.3
M / Mall
V / Vall
0.0
0.05
0.1
0.54
e/d=0.15
0.16
2R/d=0.50

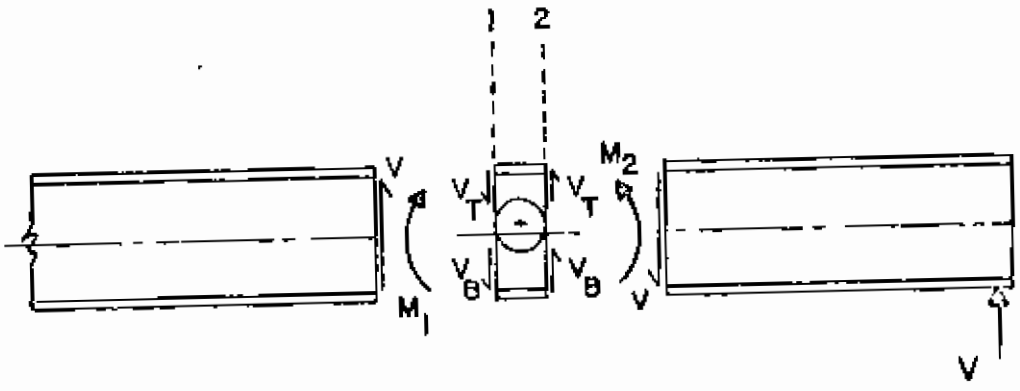

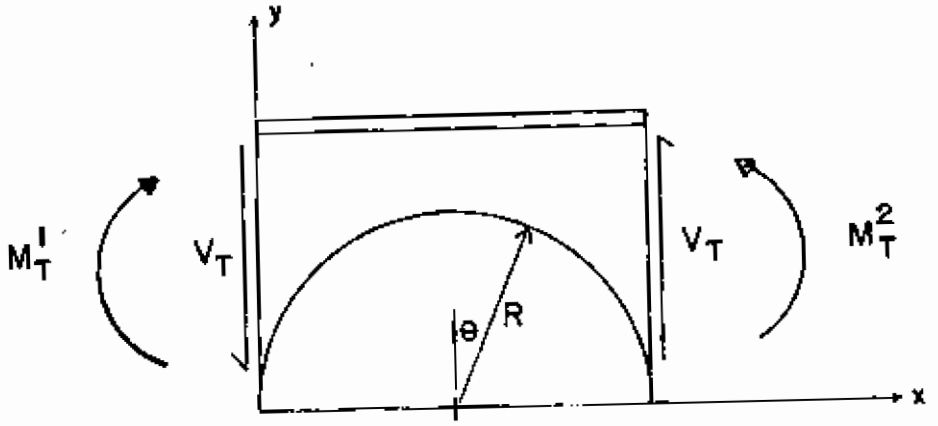

BENDING MOMENT DIAGRAM

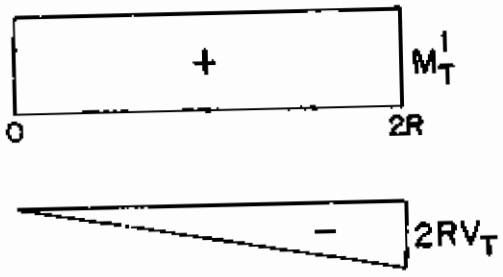

M/EI DIAGRAM

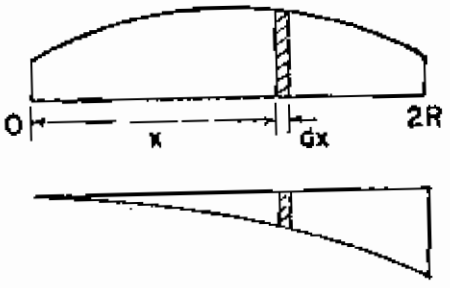

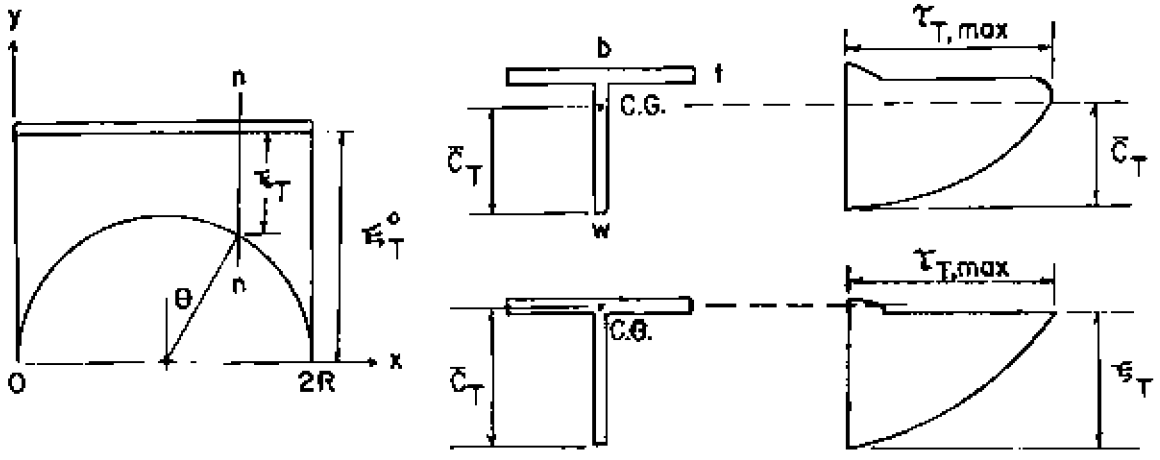
y
n
$\bar{c}_T$
$\bar{e}_T^o$
θ
n
x
0
2R
b
t
C.G.
$\bar{c}_T$
w
$\tau_{T,max}$
$\bar{c}_T$
$\tau_{T,max}$
C.G.
$\bar{c}_T$
$\bar{e}_T$

Section n-n